Hindawi
Geofluids
Volume 2020, Article ID 8881319, 22 pages
https://doi.org/10.1155/2020/8881319

Research Article

Deformation Mechanism and Control Technology of Surrounding Rock in the Deep-Buried Large-Span Chamber

Weijian Yu[1,2] **and Ke Li**[1,3]

[1]*School of Resource & Environment and Safety Engineering, Hunan University of Science and Technology, Xiangtan, Hunan 411201, China*
[2]*Hunan Provincial Key Laboratory of Safe Mining Techniques of Coal Mines, Hunan University of Science and Technology, Xiangtan, Hunan 411201, China*
[3]*College of Mining, Guizhou Institute of Technology, Guiyang, Guizhou 550003, China*

Correspondence should be addressed to Ke Li; 20120016@git.edu.cn

Received 28 May 2020; Revised 9 September 2020; Accepted 26 September 2020; Published 17 October 2020

Academic Editor: Zongqing Zhou

The selection of the support scheme for deep-buried and large-span chambers has been a severe problem in underground engineering. To further study the mechanical mechanism of large deformation, based on the repair engineering of the chambers of Pingdingshan No.6 mine in China, the field investigation, laboratory test, numerical simulation, and theoretical analysis were studied. The surrounding rock of the central substation chamber (CSC) and the main pumping chamber (MPC) were classified according to the rock mass rating (RMR) classification method, and the main factors affecting the stability of the surrounding rock of the chambers were revealed. A prediction model of mechanical parameters of the surrounding rock was established based on the Hoek-Brown failure criterion. Additionally, the prediction results were used in FLAC^{3D} to further analyze the failure of the original support scheme, and the feasibility of the restoration plan was proposed. Six key points of support technology for this kind of chamber were put forward. Comprehensive support and repair scheme, including "bolt, metal mesh, shotcrete, grouting, anchor cable, and combined anchor cable," was put forward. The engineering practice indicated that the deformation rate was less than 0.7 mm/d, which was beneficial to the long-term stability of CSC and MPC. The implementation of this restoration project can provide a reference for other similar projects.

1. Introduction

The formation process and stress action of the surrounding rock of the deep chambers are complex, showing the complex highly nonlinear mechanical characteristics. The surrounding rock has different primary stress sources in different deformation stages, including overburden pressure, loosening pressure, expansion failure pressure, expansion pressure, mining stress, and structural stress. Among them, expansion failure and the swelling pressure of clay minerals are the continuous force sources that affect the stability of the deep-buried chambers. It is challenging to realize the long-term stability of deep surrounding rock by using the existing theory and support technology. Therefore, it is necessary to classify the surrounding rock based on the deformation and failure mechanism of the surrounding rock of the chambers, take comprehensive and coordinated control measures for different types of the surrounding rock, and comprehensively consider the support countermeasures, support scheme design, support parameter determination, and construction technology measures for comprehensive analysis [1–4].

Currently, there are many pieces of research on the control of soft rock engineering. Research theories abroad mainly include classical pressure theory, collapse arch theory, new Austrian tunneling method (NATM), strain control theory, energy support theory, and numerical calculation method. The main support theories include lithology transformation theory, axial change theory, excavation system control theory, combined support theory, bolt-shotcrete-arc plate support theory, loose circle theory, primary and

secondary bearing area support theory, stress control theory, soft rock engineering support theory, and pivotal component coupling combined support theory [5–9]. Many scholars' research on in-depth engineering is mainly reflected in surrounding rock deformation and support technology [10–12], as shown in Table 1.

The current research achievements mainly focus on qualitative research on the deformation mechanism and control technology of soft rock and engineering soft rock. Since the deep underground rock mass is a complex geological body, it is still necessary to further study the deformation characteristics and mechanical mechanism of the underground engineering rock mass, especially the controllable coordination mechanism of the support structure, and the surrounding rock deformation needs to be systematically analyzed and researched. Based on the engineering background of CSC and MPC with a buried depth of 960 m, this paper attempts to explore the deformation mechanism of this deep and large-span chamber and put forward effective surrounding rock control technology; investigate the chamber's geological environment, the fracture structure characteristics of the surrounding rock, and the failure of the original support scheme in the field; analyze the development of the anatomical plane of the surrounding rock statistically; and test the mineral composition, physical property, and mechanical strength of the surrounding rock in the laboratory. According to the Hoek-Brown failure criterion, establish the prediction model of rock mechanics parameters, analyze influencing factors and control points of surrounding rock stability, put forward the control scheme, and verify them by numerical simulation and field test.

CSC and MPC were characterized by deep burial and considerable in situ stress. The surrounding rock of the chambers was characterized by severe deformation. According to the field observation, although CSC and MPC adopted the comprehensive support technology of high-strength "screw resin anchor+anchor cable+shotcrete," the surrounding rock deformation was still severe, the two sidewalls were moved close, and the floor heave was obvious. Severe deformation and damage increased the maintenance cost, resulting in significant economic losses and potential safety hazards. Therefore, according to the deformation and stability control of the chambers, the deformation mechanism analysis of the surrounding rock of the high-stress chamber was carried out. The targeted control countermeasures and new support technology were proposed, so as to achieve regular use within the service period, and play a reference role for other engineering construction.

2. General Situation and Original Support Scheme of CSC and MPC

CSC and MPC are located in the west of the No.2 Mining Area of No.6 mine. CSC is a chamber for the power supply and transformation system, and MPC is a chamber for the underground drainage system. The specific buried depth of the chamber is 960 m. The total length of CSC and MPC and their channels is 163.5 m, including a 62 m channel, a 62.5 m substation, and a 36 m pump chamber. CSC and its channel are located in the grey-black mudstone stratum, with general rock stability and no water inrush. MPC and its channel are located in grey sandstone and sandy mudstone stratum, with conventional rock stability, developed fracture, and no water inrush. The lithology of the two chambers is illustrated in Figure 1.

Figure 2 illustrates the section support; the original support of CSC and MPC adopted the joint scheme of "anchor mesh spraying+anchor cable." The anchor bolt adopted the Φ22 mm × 2600 mm high-strength resin anchor bolt with the spacing of 700 mm × 700 mm. Each hole was fitted with three resin coils of the Z2335 model, and the anchor bolt fixing force was 50 kN. The anchor cable model was Φ17.8 mm × 8000 mm, seven in each row, and the spacing was 1400 mm × 1400 mm. Each anchor cable was equipped with five coils of Z2840 resin propellant, and the anchor cable pretightening force was 100 kN, the metal mesh was made of Φ6 mm cold drawn steel wire mesh, with the mesh of 80 mm × 80 mm, mesh surface overlapping was 100 mm, shotcrete thickness was 150 mm, and strength was C20.

3. Deformation Characteristics of Surrounding Rock in CSC and MPC

3.1. Investigation on the Damage of the Support Structure. The deformation speed of the surrounding rock of the two chambers was fast; the deformation amount was substantial (as shown in Figure 3). The deformation and failure were shown in three aspects: first, the floor structure of the chamber. Floor heave had taken place in both chambers, with the maximum value of floor heave up to 1.0 m, and even the pouring concrete block structure of the floor had been arched, cracked, and separated, resulting in the chamber being unable to be used; second, the concrete sprayed in the arch had cracked and fallen off, and the anchor bolt and anchor cable pad had been squeezed; third, the arch was extruded into a peach shape, the shotcrete of the arch crown cracks and falls off, and the metal mesh was extruded, twisted, or broken; fourth, the original design was a section width of 5.8 m (excluding the thickness of the poured concrete of 300 mm); after six months, the width of the two sidewalls of the chamber had been reduced to 4.2 m. Figure 4 shows the monitoring data. The absolute deformation of the sidewall of CSC was more than 800 mm, and the deformation was still continuous.

3.2. Deformation Characteristics of the Chambers. The chambers had large deformation of the whole and full section under the action of high stress due to their low strength of surrounding rock through field monitoring and investigation. However, in terms of surrounding rock deformation itself, there are mainly the following laws:

(1) The deformation characteristics of the entire section of the surrounding rock were apparent. Depending on Figures 3 and 4, the deformation value is significant, and the absolute deformation amount reached 400-800 mm in the monitoring period. Therefore, under the action of deep-high-stress, the chambers

Table 1: Supporting theory and technology of deep-buried roadway in recent ten years.

No.	Authors	Support theory and research methods	Support technology
1.	Xie [13]	Established the spatial model of deep mining and the dynamic optimization model of the production plan and proposed the unloading technology of grave excavation face, the integrated pressure relief control strategy of the deep high-stress pillar.	Proposed the stress isolation technology of deep pressure relief curtain.
2.	He and Kanji et al. [3, 14]	Studied the deformation and failure mechanism, test methods, and equipment in deep soft rock engineering from water softening mechanism, based on the scientific definition of deep mining.	Proposed the deep soft rock large deformation design methods and control technology and developed a new constant resistance large deformation material, which is based mainly on constant resistance large deformation bolt.
3.	Li et al. [15, 16]	Established a calculation theory on the bond strength of the interface between the anchoring agent and surrounding rock.	Developed a new cementitious antiwashout grouting material and a new high-strength bolt-grouting technology.
4.	Zuo et al. [6, 17]	Theoretically derived the Hoek-Brown failure criterion based on the linear elastic fracture theory and proposed a stress gradient failure theory of surrounding rock.	Proposed uniform strength support in the deep roadway.
5.	Kang et al. [7, 18, 19]	Investigated the characteristics of deformation and failure of the entry of the tempospatial relations between heading and working faces through field study and numerical modeling.	Proposed the synergy strata control theory with bolting-modification-destressing for the roadways with 1 000 m buried depth and developed the CRMG700 rock bolt rebar with extrahigh strength.
6.	Wu et al. [20, 21]	Considered that the intersection angle of a bolt length direction and the interface of rock layers have a significant effect on the distribution and variation of axial force in bolts.	Proposed an improved support scheme for the roadway in steeply inclined geological formations, using long cables to limit severe deformation, short cables, and enclosed U-shaped steel sets to improve the ground stress state.
7.	Xie et al. [22, 23]	Deduced the equation of maximum shear stress in the deep beam structure and established the mechanical model of a truss anchor supporting roof beams.	Put forward a powerful anchor support system and anchor cable adaption technology.
8.	Yu et al. [24]	Studied the mechanism of docking long bolts and collaborative support.	Proposed a collaborative support method that uses long and short bolts.
9.	Lu et al. [25]	Studied the deformation and failure characteristics and the mechanism of "yielding support" for anchor bolts and cables.	Proposed a new "highly resistant, yielding" support system with a core of high strength, yielding bolts, and anchor cables.
10.	Tan et al. [26]	Considered the foamed concrete absorbed most of the deformations, the shrinkage of the U-shaped steel was significantly reduced.	Proposed a combined supporting system, which includes steel mesh, bolt, anchoring cable, shotcrete, compressible U-shaped steel, foamed concrete damping layer, and fractured rock cushion layer.
11.	Wu et al. [27]	Examined the influence of horizontal stress direction, pillar size between the roadways, and the excavation sequence of the roadways.	Proposed a reinforcing system that consists of high strength rock bolts and cables.
12.	Yang et al. [28]	Considered the broken and fractured rock mass near the roadway opening as ground small structure and deep stable rock mass as ground large structure.	Proposed a support technology focusing on cutting off the water, strengthening the small structure of the rock, and transferring the large structure of the rock.
13.	Wang et al. [29]	Established the governing equation for slurry seepage by utilizing the seepage mechanics theory and simulated the slurry penetration and diffusion process by utilizing the COMSOL software.	Proposed a new coupled bolting-grouting support technology with grouting anchor cable and grouting bolt.
14.	Meng et al. [30]	Plotted the safety coefficient contour of surrounding rock to judge the distribution form of the fractured zone in the roadway, which assigns rock failure criteria to calculate the rock mass unit.	
15.	Zhu et al. [31]	Developed a parametric asymmetric Voronoi block generation program by Python and implemented the parametric modeling of laminated strata in UDEC.	
16.	Zhang et al. [32]	Established the mechanical model of mining abutment pressure transmission in floor base on the theory of semi-infinite plate body in elasticity.	
17.	Gong and Li et al. [33, 34]	Investigate the spalling process in deep rectangular excavated tunnels under three-dimensional stress and considered that under the three-dimensional stress condition.	
18.	Li et al. [35]	Proposed a combined supporting scheme "double layer long bolt-mesh-shotcrete and concrete-filled steel tube."	

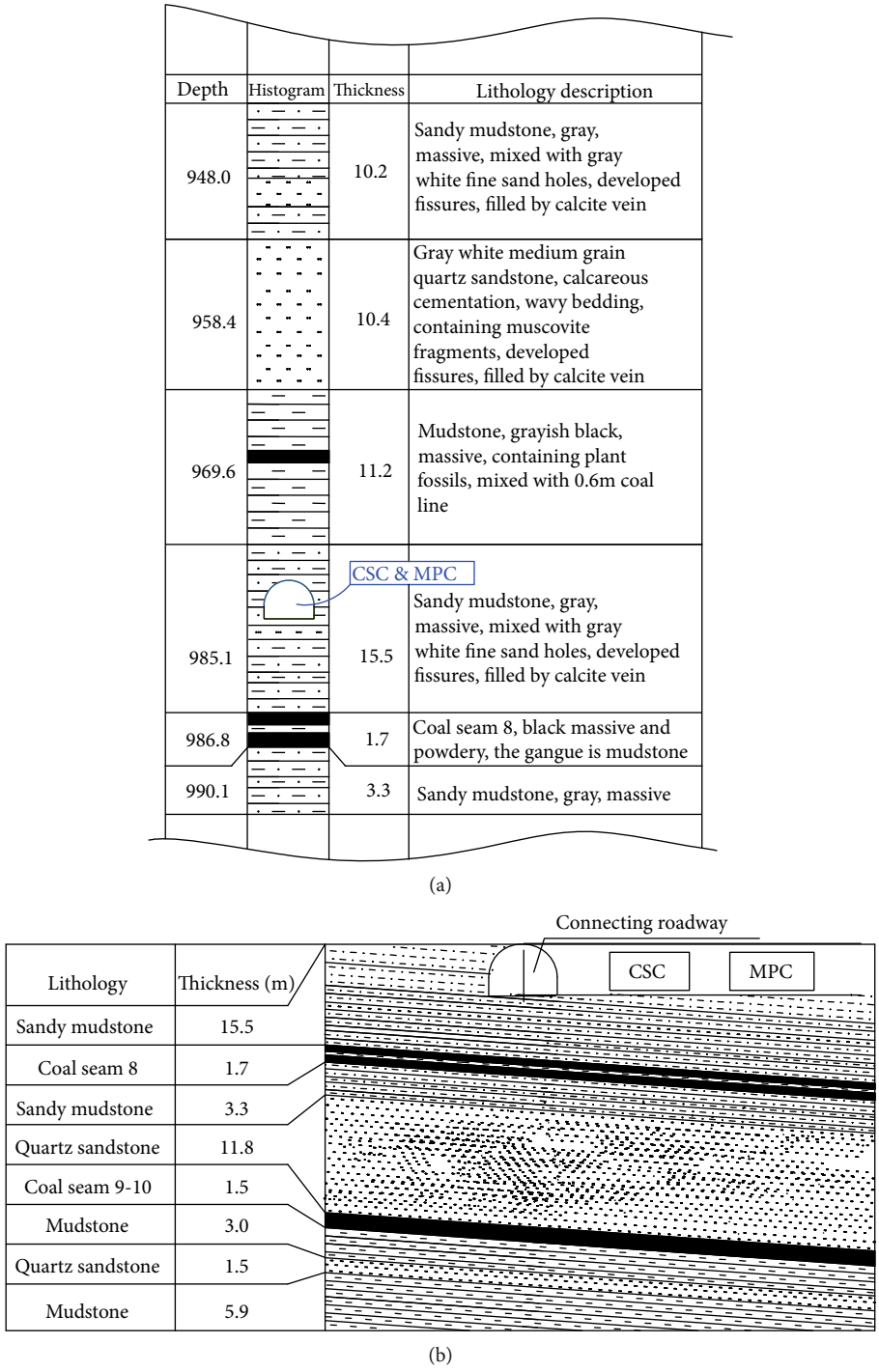

Figure 1: (a) Stratigraphic histogram of CSC and MPC. (b) Schematic diagram of floor strata of CSC and MPC.

with a large span had full section shrinkage deformation. The failure occurred at some essential parts first as the deformation becomes larger, affecting the use of the entire chamber.

(2) The internal displacement of the sidewalls was more noteworthy than that of other parts. Depending on the monitoring data and curve in Figure 4, the deformation of the straight wall of the chamber was relatively the largest, and the absolute deformation value reached 802 mm. The deformation of extra parts was relatively small, the arch of the chamber was 627 mm, the value of the floor heave was 697 mm, and the value of vault subsidence was 425 mm, respectively. Although the deformation was all-round, due to the considerable horizontal stress, which first caused the sidewalls to bulge out seriously and then caused the deformation of other parts, especially the occurrence of the tip peach shape of the vault,

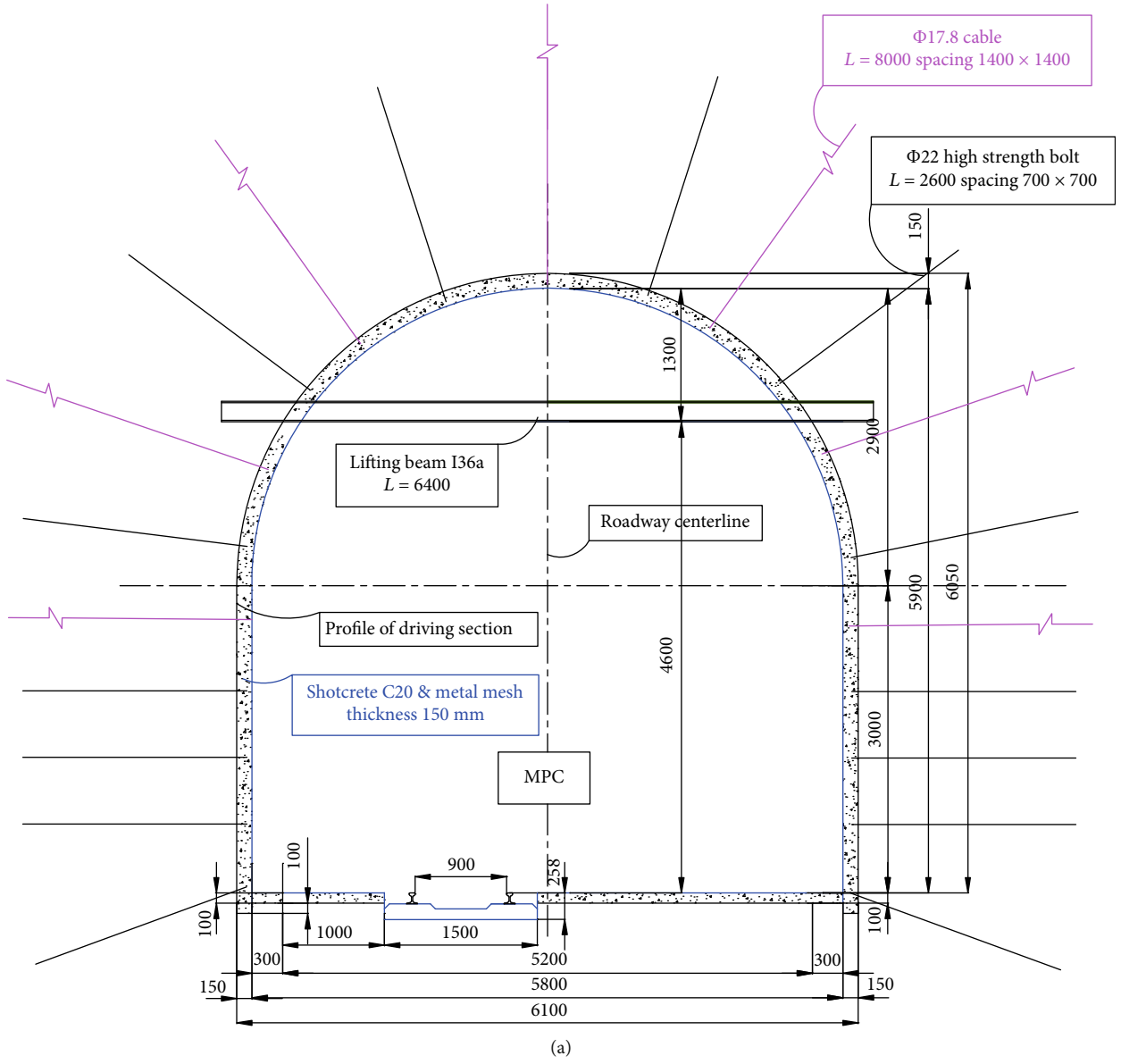

(a)

Figure 2: Continued.

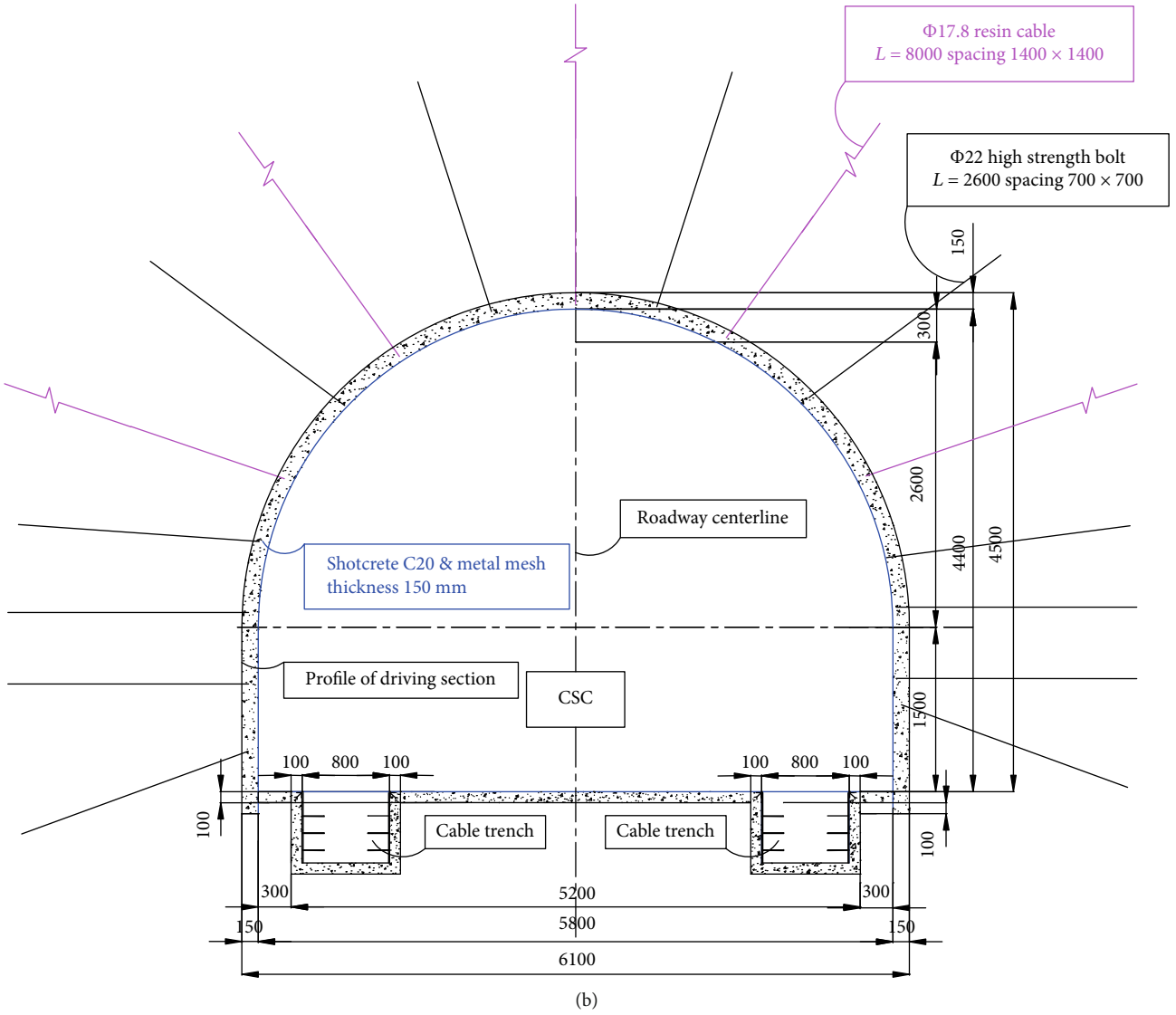

Figure 2: (a) Section and support parameters of MPC. (b) Section and support parameters of CSC.

(a) CSC (b) MPC

Figure 3: Deformation of the chambers.

which can also explain the cause of the minimum vault subsidence.

(3) The floor was damaged most seriously. Although the deformation of the sidewall was large, it was the overall internal displacement, and the degree of failure was relatively small. Under the influence of the pressure transferred from sidewalls, the concrete block structure of the floor continuously moved into the chamber space, resulting in the bulging phenomenon, which eventually caused the bending, fracture, and separation of the floor's support structure. From the field monitoring data, the floor's deformation

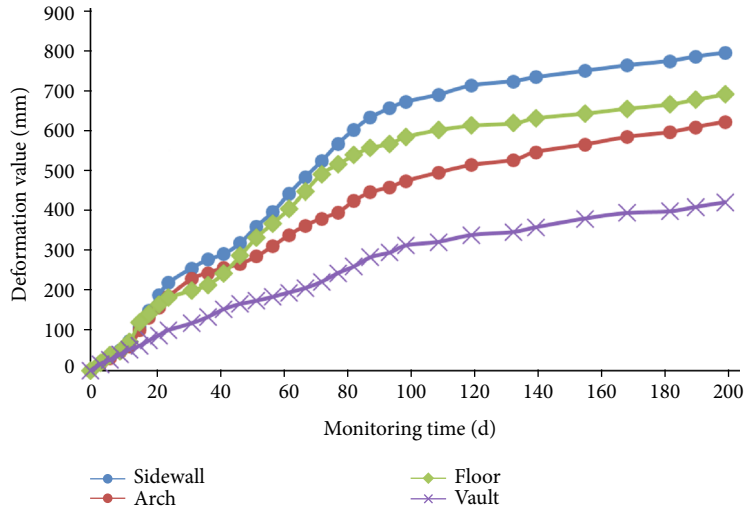

Figure 4: Deformation monitoring curve of the chambers.

value was second only to that of the sidewalls, but the damage was more prominent, as shown in Figure 3(b).

(4) Although the vault subsidence was small, the damage degree was significant. It can be seen from Figure 4 that the settlement of the vault was relatively the most minor. However, it can be seen from Figure 3 that the degree of damage is also high, which shows that the deformation of the vault was local, and local deformation is easy to cause stress concentration. Under both sides of the chamber's pressure, the vault produces a sharp peak shape, resulting in cracking and falling off of shotcrete, extrusion, distortion, or fracture of metal mesh and other damage phenomena. Therefore, it is necessary to strengthen the support of the vault.

(5) The deformation of the whole section was significant, and the duration was long. The deformation characteristics of the surrounding rock of the chamber were also reflected in the deformation value. Only within 6 months after the completion of the excavation of the chambers, the maximum deformation value reached 802 mm; the width of the cross-section was equivalent to 1.6 m reduced. The relative displacement of the roof-floor reached 1.1 m; the usable area of the whole cross-section was significantly reduced. Besides, the deformation of surrounding rock continues to increase after the monitoring period of 6 months, and the deformation speed remained at 1 mm/day, which was an unstable state.

3.3. Fracture Structure Characteristics of the Surrounding Rock. Three boreholes ($l = 10$ m) were drilled in the sidewalls and the roof for peeping observation; Figure 5 shows the results. The longitudinal fracture development range of the surrounding rock mass at the borehole locations was uniform and consistent, indicating that the rock mass from the hole opening to the hole was relatively loose and the fracture was developed. Still, the rock mass integrity was better after 6.0 m. Therefore, fracture expansion of the chamber surrounding rock was synchronous, showing the overall deformation law, and the loosening circle was about 5.5-6.0 m.

4. Mechanical Properties and Stability Evaluation of Surrounding Rock

4.1. Mineral Composition of Surrounding Rock. Two rock specimens were collected in CSC, and their mineral composition was analyzed by an X-ray diffractometer; Table 1 shows the results. According to the analysis results, the proportion of kaolinite, montmorillonite, and other clay minerals in the surrounding rock of chambers is relatively high, especially the content of kaolinite that reaches 79.4%. Also, there are numerous montmorillonite minerals, so the surrounding rock is natural to soften, muddy, and expand when encountering water, which affects the chamber's stability.

4.2. Rock Mechanics Test. The rock specimens were taken from the CSC channel, including two typical rocks: siltstone of the roof and sandy mudstone of the floor. The density of rock specimens was determined, as shown in Table 2.

For the tensile strength of the rock block, the indirect method (splitting tensile method) was used to test. The specific specification of the test piece is a cylinder with diameter × height = 5 cm × 5 cm; Table 3 shows the test results. The uniaxial compressive strength was tested by RMT-150. Table 4 shows the results.

4.3. Joint Investigation of Surrounding Rock. The joints and fractures of the surrounding rock were investigated on site. The particular line observation method was adopted for the investigation method [36]. This area is dominated by argillaceous sandstone, with relatively developed joint fissures; the integrity of the rock mass is functional, with a small amount of fillings, mainly argillaceous minerals. The fracture structure surface spacing is about 0.15~1.0 m, generally more than 3 groups, mostly in elastic-plastic medium, with general

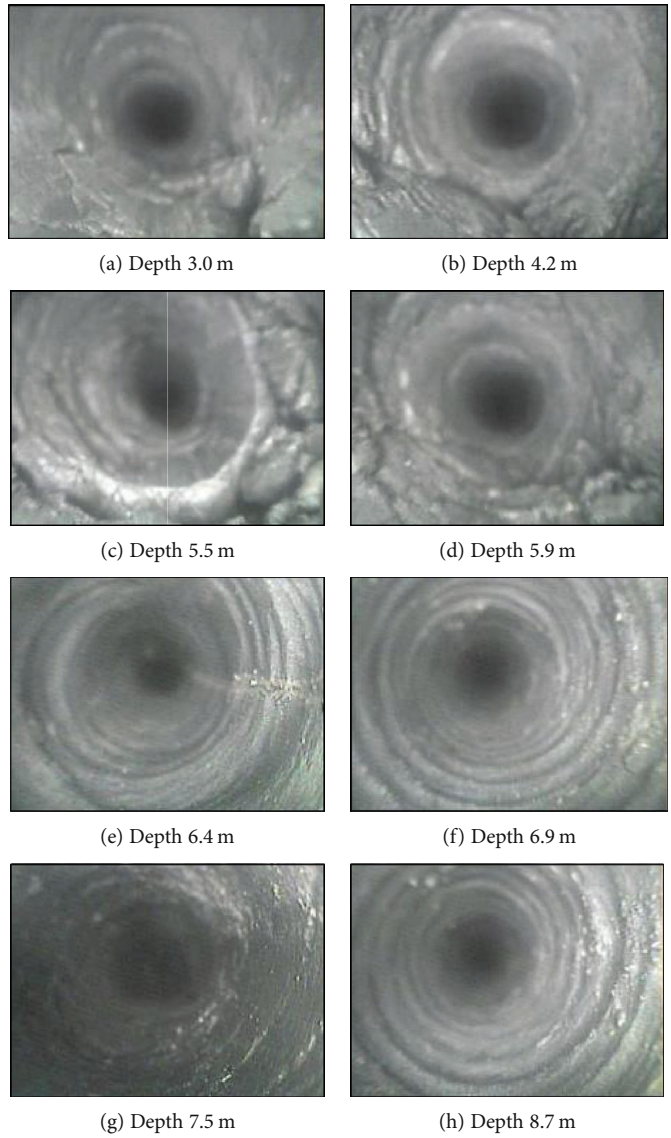

(a) Depth 3.0 m (b) Depth 4.2 m

(c) Depth 5.5 m (d) Depth 5.9 m

(e) Depth 6.4 m (f) Depth 6.9 m

(g) Depth 7.5 m (h) Depth 8.7 m

Figure 5: Borehole observation photos.

Table 2: Mineral composition of surrounding rock of chambers.

Mineral name	Quartz (SiO_2)	Pearl stone ($Mg_3Si_2O_5(OH)_4$)	Kaolinite ($Al_2Si_2O_5(OH)_4$)	Serpentine ($Al_2Si_2O_5(OH)_4$)	Montmorillonite ($Na_{0.3}Al_4Si_6O_{15}(OH)_64H_2O$)
Mineral content	7.5%	5.2%	79.4%	3.7%	4.5%

stability. According to the statistics of the spacing of the joints and other structural planes in the surrounding rock of the chamber, the volume joints of the rock mass J_v are 3-10 joints/m^3, with an average of 6 joints/m^3. It is noted that the maximum spacing of joints is 60 cm, the minimum is less than 1 cm, and the total average is about 26 cm. The integrity coefficient K_v of surrounding rock is about 0.8, with functional integrity, the number of joint groups is 2-3, the roughness of the joint surface is generally plane roughness, the filler is argillaceous mineral and talc, and the thickness of filler is between 2 and 15 cm.

4.4. Analysis of Calculation Parameters of Surrounding Rock

4.4.1. Prediction Theory and Method of Rock Mechanical Parameters. There are many methods to predict the characteristic parameters of the rock mass, including mechanical tests, displacement inversion, and pattern recognition. The most practical and useful functions are the linear Mohr-Coulomb criterion and the nonlinear Hoek-Brown criterion [6, 37]. Therefore, to overcome the difficulties of the rock mechanics parameter analysis method as much as possible, based on field investigation, the Hoek-Brown failure criterion

Table 3: Determination of rock mass density.

Lithology	Number	D (mm)	H (mm)	m (kg)	ρ (t/m^3)	ρ_1 (t/m^3)
Roof siltstone	1-1	48	70	0.33	2.61	2.48
	1-2	48	68	0.34	2.76	
	1-3	48	72	0.32	2.46	
	1-4	48	71	0.31	2.41	
Sandy mudstone of floor	2-1	48	64	0.29	2.51	
	2-2	48	65	0.27	2.30	
	2-3	48	57	0.25	2.43	
	2-4	48	61	0.26	2.36	

Note: D is diameter; H is height; m is weight; ρ is density; ρ_1 is average density.

Table 4: Rock tensile test results.

Number	Size		σ_t (MPa)	σ_t' (MPa)
	D (mm)	H (mm)		
2-1	48	64	4.21	4.07
2-2	48	65	4.61	
2-3	48	57	3.22	
2-4	48	61	4.23	

Note: σ_t is the tensile strength; σ_t' is the average tensile strength.

is used to predict the mechanical parameters of deep large-span chamber (e.g., CSC and MPC) surrounding rock, and the stability analysis is carried out.

Since the Mohr-Coulomb yield criterion is a linear function, Evert Hoek and E. T. Brown proposed a nonlinear failure criterion based on a large number of engineering practices, which is closer to the reality:

$$\sigma_1 = \sigma_3 + \sigma_{ci}\left(m_i \frac{\sigma_3}{\sigma_{ci}} + s_i\right)^{0.5}, \tag{1}$$

where σ_1 and σ_3 are the maximum and minimum principal stress, σ_{ci} is the uniaxial compressive strength of the rock mass, and m_i and s_i are the material constants of Hoek-Brown failure criterion, respectively, which can be estimated according to the RMR value. For the rock mass, $s_i = 1$.

Based on the above research, Hoek and Brown extended the criterion function of Equation (1) and put forward the general Hoek-Brown failure criterion as follows:

$$\sigma_1 = \sigma_3 + \sigma_{ci}\left(m_b \frac{\sigma_3}{\sigma_{ci}} + s_i\right)^{a}, \tag{2}$$

where m_b is the material parameter of rock mass and s_i and a are the constants of rock mass, respectively.

Equation (2) can better reflect the failure ($a = 1/2$) of most good quality rock masses, but it does not apply to poor quality rock masses. Therefore, Equation (3) is used instead to express

$$\sigma_1 = \sigma_3 + \sigma_{ci}\left(m_b \frac{\sigma_3}{\sigma_{ci}}\right)^{a}. \tag{3}$$

For the parameters m_b, s_i, and a of the estimated engineering surrounding rock properties, when RMR > 25, it can be concluded that

$$m_b = m_i \exp\left(\frac{\mathrm{RMR} - 100}{14}\right), \tag{4}$$

$$s_i = \exp\left(\frac{\mathrm{RMR} - 100}{6}\right). \tag{5}$$

When RMR < 25, Equations (4) and (5) are not applicable, and a new indicator GSI is introduced to determine the values of m_b, s_i, and a as follows:

$$m_b = m_i \exp\left(\frac{\mathrm{GSI} - 100}{28 - 14D}\right), \tag{6}$$

$$s_i = \exp\left(\frac{\mathrm{GSI} - 100}{9 - 3D}\right), \tag{7}$$

$$a = \frac{1}{2} + \frac{1}{6}\left(e^{-\mathrm{GSI}/15} - e^{-20/3}\right), \tag{8}$$

where m_i is the material parameter of complete rock; D is the influence coefficient of engineering factors (mainly considering the reduction of rock property parameters caused by rock disturbance caused by excavation blasting and stress release). Therefore, the value is between 0 and 1, i.e., for the original rock state, the value is 0; for the fully disturbed rock mass, the value is 1; GSI is the geological strength index.

GSI indicators can be calculated by RMR:

$$\text{when RMR} > 23, \mathrm{GSI} = \mathrm{RMR} - 5, \tag{9}$$

$$\text{when RMR} < 23, \mathrm{GSI} = 9 \cdot \ln\left(\frac{\mathrm{RQD}}{J_n} \cdot \frac{J_r}{J_a}\right) + 44, \tag{10}$$

where RQD is the rock quality index, %, J_r is the joint roughness coefficient, J_n is the joint group coefficient, and J_a is the joint strength reduction coefficient.

The most prominent feature of the Hoek-Brown failure criterion is to consider the influence of engineering factors on rock mass characteristic parameters. Hoek and Brown also give the typical values of m and s of the disturbed and

undisturbed rock mass. Since the Mohr-Coulomb failure criterion is still used in most of the numerical software, the equivalent rock parameters of the Mohr-Coulomb model, internal friction angle φ' and cohesion c', can be obtained through the average linear relationship fitting of the relationship curve given in Equation (3) within the corresponding stress range. The equation is

$$\phi' = \sin^{-1}\left[\frac{6am_b\left(s + m_b\sigma'_{3n}\right)^{a-1}}{2(1+a)(2+a) + 6am_b\left(s + m_b\sigma'_{3n}\right)^{a-1}}\right], \quad (11)$$

$$c' = \frac{\sigma_{ci}\left[(1+2a)s + (1-a)m_b\sigma'_{3n}\right]\left(s + m_b\sigma'_{3n}\right)^{a-1}}{(1+a)(2+a)\sqrt{1 + \left[6am_b\left(s + m_b\sigma'_{3n}\right)^{a-1}\right]/[(1+a)(2+a)]}}, \quad (12)$$

where $\sigma'_{3n} = \sigma'_{3\,\max}/\sigma_{ci}$.

For a given normal stress σ, the shear strength τ can be calculated by the equivalent internal friction angle φ' and cohesion c', that is,

$$\tau = c' + \sigma \tan\phi'. \quad (13)$$

The relationship between the maximum and minimum principal stresses is as follows:

$$\sigma'_1 = \frac{2c'\cos\phi'}{1-\sin\phi'} + \frac{1+\sin\phi'}{1-\sin\phi'}\sigma'_3. \quad (14)$$

When the stress of the excavation boundary reaches σ_c, the rock mass begins to break, and gradually expands into the biaxial compression state. However, it is necessary to consider the overall strength of the rock mass rather than the local asymptotic expansion failure. For example, when considering the strength of the pillar, it is necessary to consider the strength of the whole pillar rather than the progressive failure process of the pillar. Therefore, Hoek and Brown proposed the concept of overall rock mass strength. According to the Mohr-Coulomb failure criterion, the equation of c' and φ' is as follows:

$$\sigma'_{cm} = \frac{2c'\cos\phi'}{1-\sin\phi'}. \quad (15)$$

When $\sigma_t < \sigma'_3 < \sigma_{ci}/4$, according to the calculation equation of rock mass parameters in Hoek-Brown failure criterion:

$$\sigma'_{cm} = \sigma_{ci}\frac{[m_b + 4s - a(m_b - 8s)](m_b/4 + s)^{a-1}}{2(1+a)(2+a)'}. \quad (16)$$

According to GSI, the equation of deformation modulus of rock mass can be determined as follows:

$$E_m = \left(1 - \frac{D}{2}\right)\sqrt{\frac{\sigma_{ci}}{100}}\cdot 10^{[(\mathrm{GSI}-10)/40]}\,(\sigma_{ci} \le 100\,\mathrm{MPa}), \quad (17)$$

$$E_m = \left(1 - \frac{D}{2}\right)10^{[(\mathrm{GSI}-10)/40]}\,(\sigma_{ci} > 100\,\mathrm{MPa}). \quad (18)$$

The blasting and stress release of rock excavation will inevitably affect the rock characteristics. It is necessary to consider the influence of engineering activities on rock mass characteristics. Therefore, according to the Hoek-Brown failure criterion, an engineering influence factor D is introduced to quantify the influence degree of excavation on rock property parameters.

4.4.2. Chamber Surrounding Rock Parameter Prediction and Stability Analysis. The mechanical engineering parameters of the surrounding rock of the chamber can be obtained according to the Hoek-Brown failure criterion strength. The calculation and statistical results are presented in Table 5. The stability of the surrounding rock of CSC and MPC is general or deviation according to the consequences of these parameters. Referring to the RMR method, the RMR value of the surrounding rock of MPC is 54-61 (class III); the RMR value of the surrounding rock of CSC is 35-42 (class IV), basically belonging to class III or class IV. However, from the experimental and predicted results of rock mechanics parameters, if this kind of surrounding rock is in the condition of low stress, its stability is well. However, the burial depth of CSC and MPC is nearly 1000 m, the original rock stress is high, and the vertical stress can reach 25 MPa. Besides, the mining area is affected by the structural stress, resulting in severe deformation of high-strength rock, especially for the chamber with a large span; the full section deformation is more prominent.

5. Control Principle and Technology in Deep Large-Span Chambers

5.1. Factors Influencing the Stability of Surrounding Rock. According to the comprehensive analysis of the stress environment and lithology of the surrounding rock, the main reasons for CSC and MPC failure are as follows:

(1) The strength of the surrounding rock is weak, the joint fissures are developed, and the self-stability is poor. According to the above analysis results, the surrounding rock of the chamber contains kaolinite and montmorillonite and other mineral components, especially weak rock and argillaceous mineral components, which have an essential impact on the nature and intensity of deformation and failure of the chamber. At the same time, the deformation and failure of the surrounding rock are closely related to the structural characteristics of the surrounding rock and the failure state of the rock mass itself, among which the bedding and joints are the most influential and the most common, which will cause

Table 5: Uniaxial compressive strength test results.

Lithology	Number	σ_c (MPa)	E (MPa × 10^4)	μ	σ_{c1} (MPa)	E_1 (MPa × 10^4)	μ_1
Roof siltstone	1-1	97.23	24.45	0.15	80.28	25.63	0.25
	1-2	81.74	17.29	0.19			
	1-3	74.04	24.33	0.28			
	1-4	68.12	36.44	0.39			
Sandy mudstone of floor	2-1	43.91	12.39	0.47	38.66	15.39	0.40
	2-2	39.37	15.86	0.39			
	2-3	34.12	14.67	0.41			
	2-4	37.24	18.64	0.33			

Note: σ_c is compressive strength; E is the modulus of elasticity; μ is Poisson's ratio; σ_{c1} is the average compressive strength; E_1 is the average modulus of elasticity; μ_1 is the average Poisson's ratio.

the expansion of the cracks under the action of high stress and quickly form new microcracks.

(2) The buried depth is considerable, and the ground stress is significant. The buried depth of CSC and MPC is 960 m, and the vertical stress is 25 MPa. In addition to the effect of horizontal structural stress, the engineering force has more apparent damage to the surrounding rock of the chamber when it is excavated. According to the stability analysis results, the stability level of the two chambers is in class III to IV. Therefore, from the large deformation of the chamber, the surrounding rock mainly belongs to high stress engineering soft rock, which is mainly the effect of engineering stress, and the effect of rock lithology is relatively small.

(3) The deformation mechanism is unclear, and the supporting parameters are unreasonable. The original support parameters cannot effectively control and adapt to the deformation of the surrounding rock of the chamber. The most crucial thing about bolt support is to form a reinforcement ring, and this reinforcement ring should also have a high bearing capacity. If the anchor end (i.e., the whole bolt and anchor cable) is located in the loose ring, its anchoring effect is challenging to play.

(4) The structural stress is significant, and the floor heave is prominent. Under the action of high stress, especially horizontal stress, the surrounding rock of the chamber takes the chamber floor as the free surface along the goaf, and the soft and broken rock mass of the floor is squeezed by horizontal stress and flows into the chamber, forming the chamber floor heave. In this way, with the increasing deformation of the floor, the floor's supporting structure breaks and fails. With the two sidewalls also squeezed in, the arch crown becomes a peach shape, the concrete cracks, and the spalling, and other phenomena are caused.

5.2. Principles of Controlling Surrounding Rock. The main idea is to improve the strength of the surrounding rock of internal structure as soon as possible and prevent the infinite relative displacement of concentrated stress in the surrounding rock. Therefore, according to the failure condition and stability category of the chambers, the following control principles are proposed:

(1) Improve the initial support stiffness and strength of the support system. Due to the low strength of the structural plane, the discontinuous deformation is before the continuous deformation after the excavation of underground engineering. Therefore, to control the deformation of the surrounding rock, it is necessary to improve the preliminary support stiffness and strength of the support system significantly, effectively control the discontinuous deformation of the surrounding rock, and maintain the integrity of the surrounding rock. At the same time, it is required that the support system should have enough elongation, allowing the surrounding rock of the chamber to have large continuous deformation, so that the high stress can be released, especially emphasizing "first rigid, then soft, then rigid, first resistant, then resistant," to maintain the integrity of the surrounding rock to the maximum extent, and to minimize the reduction of the strength of the surrounding rock.

(2) Give full play to the bearing function of the rock mass in the deep unchanging position. To make the surrounding rock in the compression state, inhibit the occurrence of bending deformation, tensile, and shear failure of the surrounding rock and make the surrounding rock become the main bearing body. Therefore, it is necessary to find the deep stable rock mass as the bearing support point, so that the anchor rod and anchor cable can form a prestressed bearing structure with high rigidity in the anchorage area, prevent the separation of the rock layer outside the anchorage area, improve the stress distribution in the deep part of the surrounding rock, and significantly improve the support effect.

(3) Expand the bearing area of the support system, especially the spread of anchor and cable prestress. In the support design, the reasonable prestress should be determined according to the surrounding rock conditions of the chamber, and the effective diffusion of

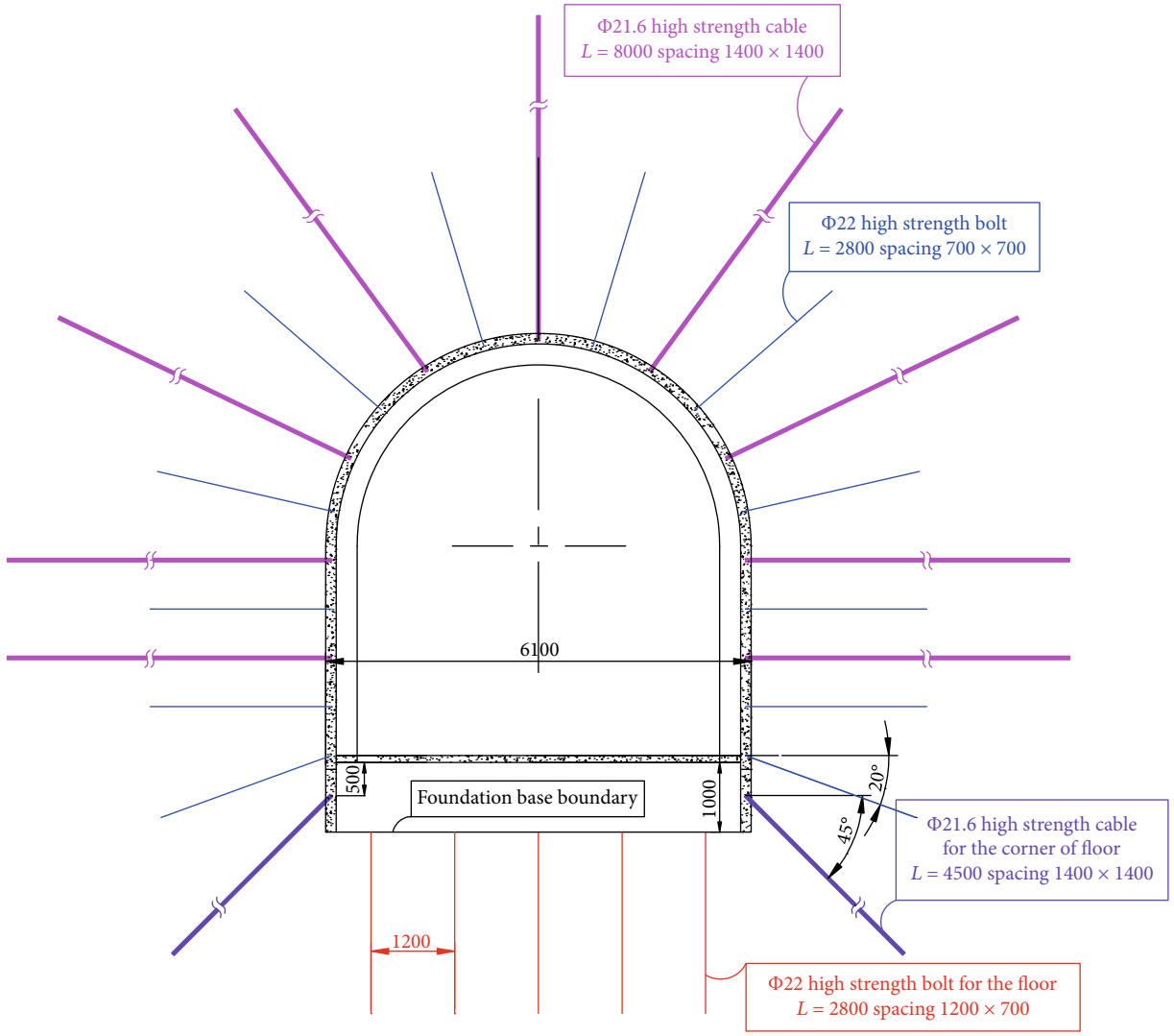

Figure 6: Deep hole (6 m) grouting scheme.

prestressing is the key to the support design. The prestress of a single bolt (an anchor cable) must be diffused to the surrounding rock farther away from the bolt through supporting plate, steel belt, metal mesh, and other components. Particularly for the surface of the chamber, even if a small support force is applied, the deformation and damage of the surrounding rock will be restrained, and the integrity of the roof will be maintained. Therefore, it is essential to give full play to bolt (an anchor cable) supporting plate, steel belt, and metal mesh in the prestressed support system.

(4) Accurately grasp the critical support stiffness of the support system. There is vital support stiffness in the bolt, anchor cable, and U-shaped steel frame. How to effectively combine several support structures and form a coordinated bearing system with surrounding rock also determines the control effect to a large extent. If the rigidity of the support system is less than the critical support rigidity, the surrounding rock will be in the state of deformation and instability for a long time; on the contrary, if the stiffness of the support system reaches or exceeds the critical support rigidity, the surrounding rock deformation will be adequately restrained, and the chamber will be in the state of long-term stability. In the actual operation process, the decisive factor determining the critical support stiffness is the prestress of the anchor bolt (an anchor cable). Therefore, as long as the anchor bolt (an anchor cable) reaches the critical prestress value, it can effectively control the deformation and separation of surrounding rock, and the stress of the support structure has little change.

(5) To use the combined support structure. In the initial support, the combination of high prestressed anchor cable and the secure anchor bolt is used first. The deformation and damage of surrounding rock can be effectively controlled by one support as far as possible, and secondary support and chamber

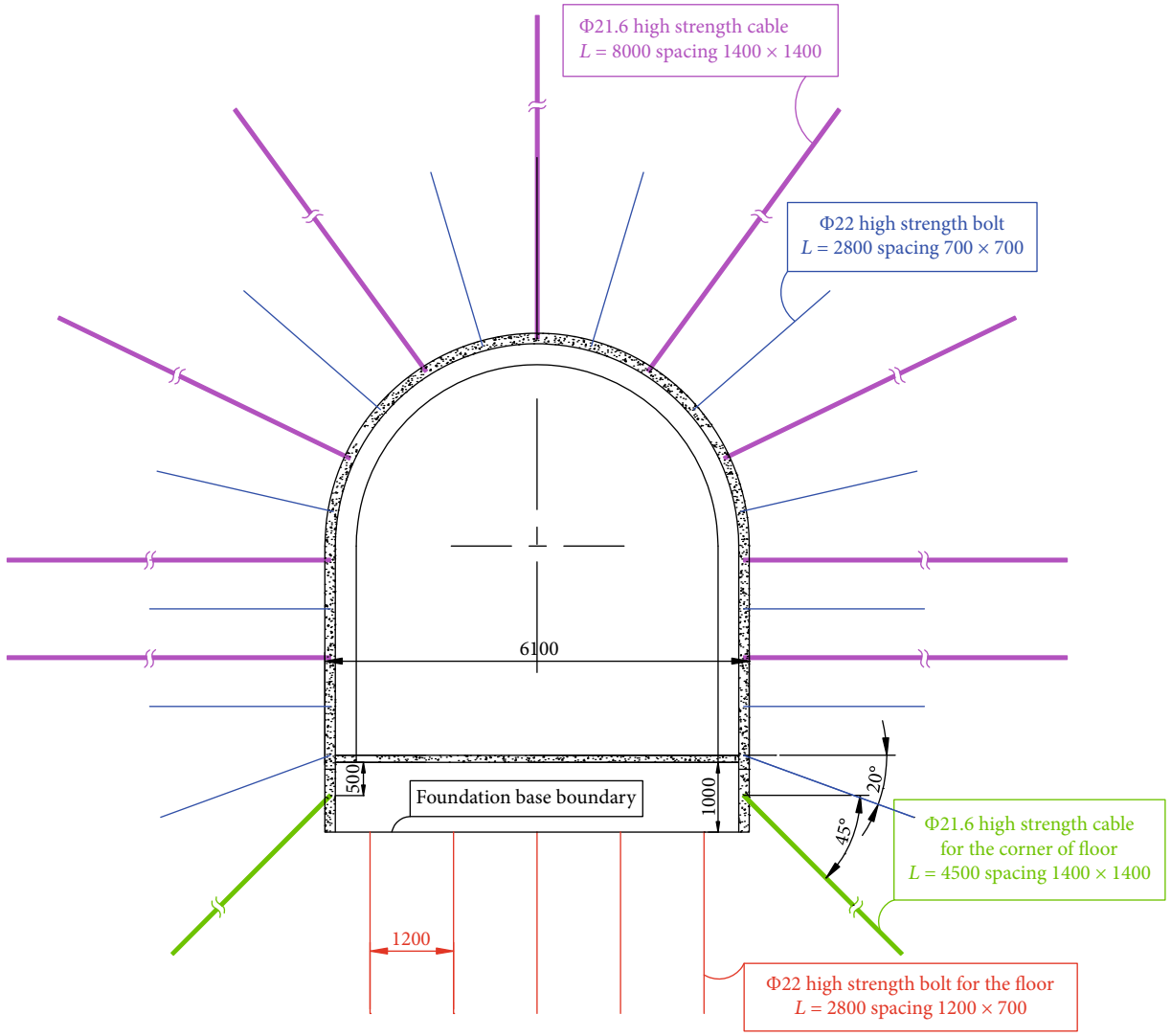

Figure 7: Full section support scheme after repair.

maintenance can be avoided. To improve the integrity and bearing capacity of the rock mass, grouting should be carried out as soon as possible in the initial support, so that the surrounding rock of the chamber can form an "inside and outside" arch bearing structure with high bearing capacity and functional integrity in the loose circle, thus significantly improving the strength and integrity of the surrounding rock.

(6) Improve the deformation resistance of the floor. According to the large deformation of the chamber, the floor heave is the preliminary stage that causes the whole chamber to lose stability. Therefore, improving floor strength is the key to controlling the stability of the entire chamber section. In the concrete design and construction, strengthen the antideformation structure of the floor and make full use of the effect of the floor "beam" or "reverse bottom arch" to resist the pressure and deformation of the surrounding rock and to maintain the stability of the whole section of the chamber. Besides, the anchoring function of anchor or cable should also be played, and the rock strata moving to the chamber space should be anchored in the stable rock stratum deep in the floor, which can effectively restrain part of the deformation.

5.3. Scheme Design of Controlling of CSC and MPC. According to the control principle determined above, the comprehensive support mode of "bolt, metal mesh, shotcrete, grouting, anchor cable, and combined anchor cable" is proposed for the whole chamber section. The specific repair process is as follows: initial shotcrete→grouting at all sections of surrounding rock→lane expansion→combined support of anchor and shotcrete mesh→full section anchor cable support→combined grouting anchor cable→shotcrete. The determination of grouting hole and anchor cable support parameters is mainly based on the peep results of fracture development in the rock mass (Figure 5). Because the rock mass with the depth of 5.5-6.0 m is relatively loose and

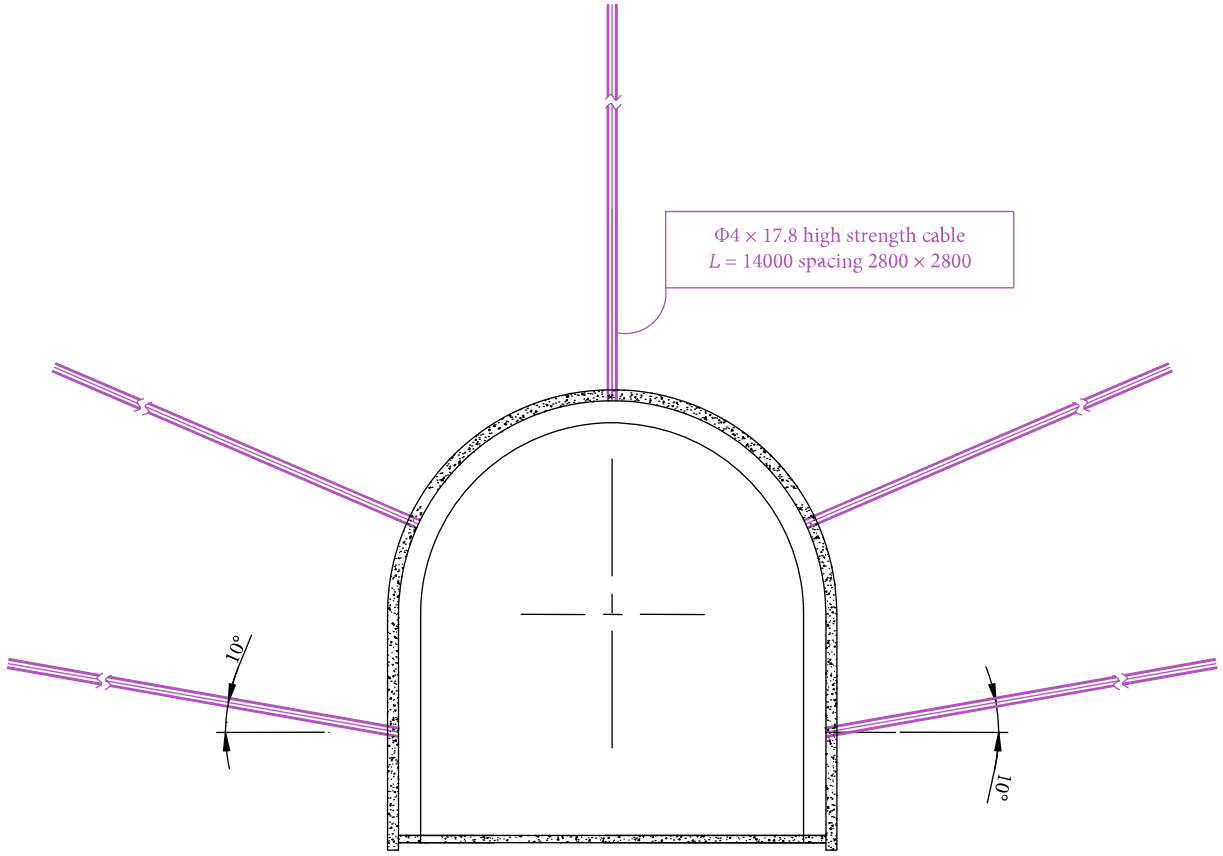

Figure 8: Combined grouting anchor cable support and parameters.

Table 6: Prediction results of chamber rock mass parameters (project type: chamber; $H = 960$ m).

Project name	Uniaxial compressive strength $\boldsymbol{R}_{cm}$/MPa	Uniaxial tensile strength $\boldsymbol{R}_{tm}$/MPA	Deformation modulus E_m/GPa	Cohesion C_m/MPa	Friction angle φ_m/(°)
MPC	8.57	2.36	2.23	1.31	29.73
CSC	4.96	1.43	1.73	0.97	19.34

fracture developed, the rock mass integrity is functional after 6.0 m, which shows that the loosening circle is about 5.5-6.0 m. The following takes the MPC as an example to illustrate the specific control parameters:

(1) Grouting design of surrounding rock before roadway expansion: the length of the grouting hole is determined as 6 m; the spacing between the grouting holes on the vault is 3000 mm × 2000 mm; the spacing on the sidewalls is 2000 mm × 2000 mm; the spacing on the floor is 2400 mm × 2000 mm. The specific layout is shown in Figure 6. The grouting material is cement water glass double-liquid slurry

(2) Bolt support parameters: the bolt support parameters of the two sidewalls and the vault still adopt the original support form:

Two sidewalls and vault: the anchor bolt is made of Φ22mm, $L = 2800$ mm left-hand nonlongitudinal high-strength screw steel, and the anchor material is BHRB500 left-hand nonlongitudinal screw steel. Three rolls of K2840 resin anchoring agents are used for each anchor rod, with the pretightening force not less than 100 kN, and the row spacing between anchor rods is 700 mm × 700 mm, as shown in Figure 7. The whole section is hung with metal mesh and steel ladder beam, with the metal mesh of Φ6 mm and mesh of 80 × 80 mm. The metal mesh joint must be tightened with an anchor rod and reinforced ladder beam close to the rock's surface. The length of the joint between nets shall not be less than 100 mm. The reinforced ladder beam is made of 12 mm diameter round steel by welding.

Floor: the anchor rod is made of Φ22 mm, $L = 2800$ mm left-hand nonlongitudinal high-strength screw steel, and the anchor material is BHRB 500 left-hand nonlongitudinal screw steel. Three rolls of K2840 resin anchoring agent shall

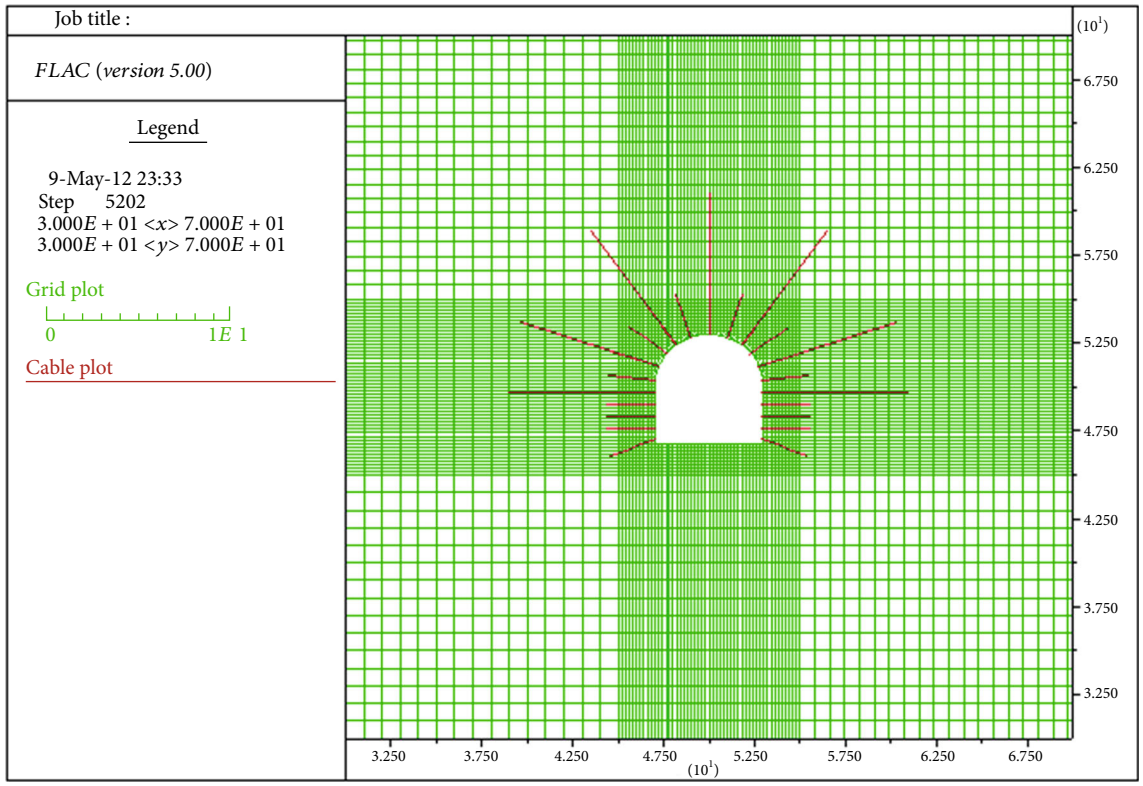

Figure 9: Numerical calculation model of the original support scheme of MPC.

be used for each anchor bolt, with the pretightening force not less than 100 kN, and the row spacing between anchor bolts is 1200 mm × 700 mm, as shown in Figure 7. The anchor rod on the floor is attached by a reinforced ladder beam to form a whole.

(3) Anchor cable support: the anchor cable is Φ21.6 mm and made of steel strand. The length of the anchor cable is $L = 8.0$ m (including the length of the anchor cable at the floor corner that is 4500 mm). The design is shown in Figure 7, with the spacing of 1400 mm and a row spacing of 1400 mm. Resin end anchorage has an anchorage length of 1600 mm. Five rolls of Z2840 resin agent shall be used for each anchor cable, and the preload shall not be less than 100 kN. Two base plates overlap the anchor cable base plate, the specifications of which are 350 mm × 350 mm × 10 mm and 150 mm × 150 mm × 10 mm square base plates, with the large base plate on the top and small base plate on the bottom. The anchor cable at the bottom angle is arranged at an angle of 45°, as showed in Figure 7

(4) Combined grouting anchor cable: each group of combined grouting anchor cables is woven by four Φ17.8 × 14000 mm anchor cables, with the spacing of 2.8 × 2.8 m and each row of five cables. The length of a grouting anchor cable is 14 m, which is divided into anchorage section (7.5 m), free section (6 m), and expansion section (0.5 m). The whole bunch of anchor cable is composed of a steel strand, guide cap, plastic sleeve, support frame, and exhaust pipe. The anchor cable tray is made of 25 channel steel and 20 mm steel plate. The grouting anchor cable shall be tensioned, and the pretightening force shall not be less than 120 kN. The grouting material is cement water glass double-liquid slurry. The specific layout and parameters are shown in Figure 8

6. Application Effect of the Designed Support Method

6.1. Numerical Simulation Calculation. The corresponding numerical analysis model is set up according to the engineering geological data to analyze the reasons of surrounding rock failure and compare the supporting effect of different schemes. FLAC 2D software is used to analyze the plane strain and deformation of the surrounding rock of the chamber, and the surrounding rock is regarded as a layered elastic isotropic medium. The size of the model is 100 m × 100 m. The displacement boundary is taken at the left, right, and bottom of the calculation model, while the stress boundary is taken at the upper part, whose stress is the self-weight stress of the upper overburden. According to the actual surrounding rock medium, the upper boundary stress is 25 MPa. As the horizontal tectonic stress caused by deep structure is significant, the lateral pressure coefficient (λ) is set as 1.3. According to the typical histogram and geological data, the parameters can be preliminaries determined, as shown in Table 6.

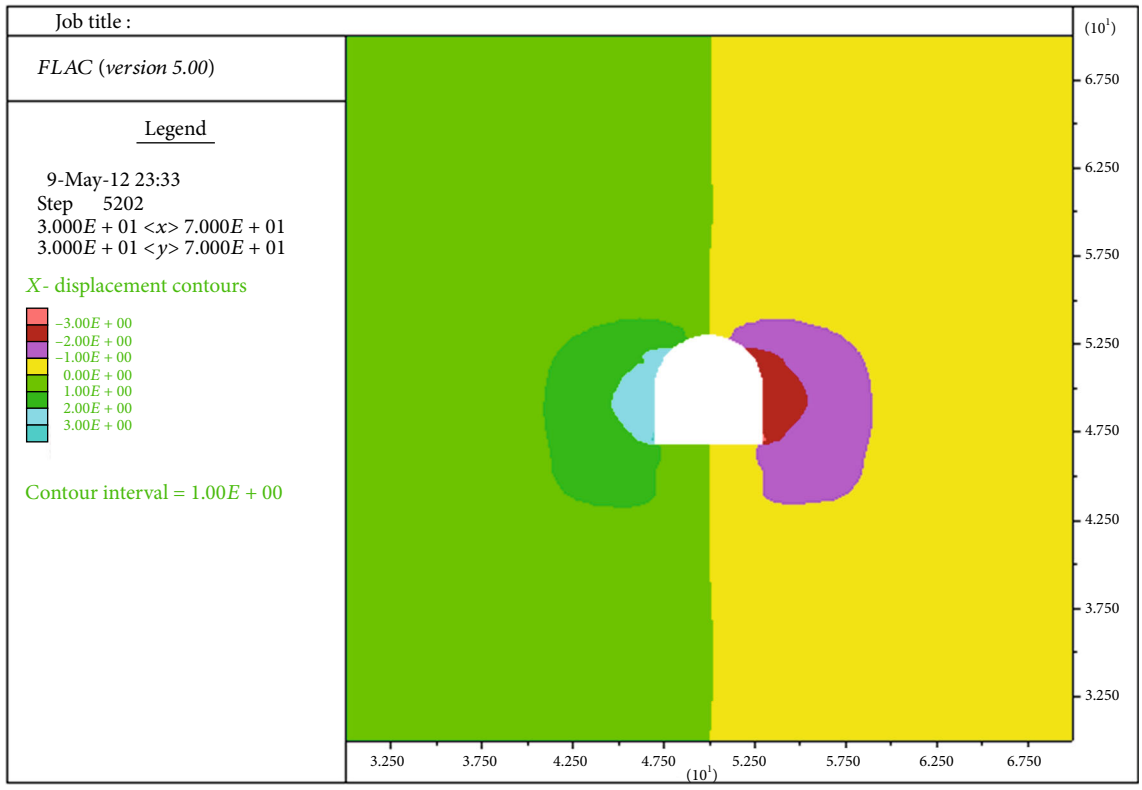

Horizontal displacement

(a) Horizontal displacement

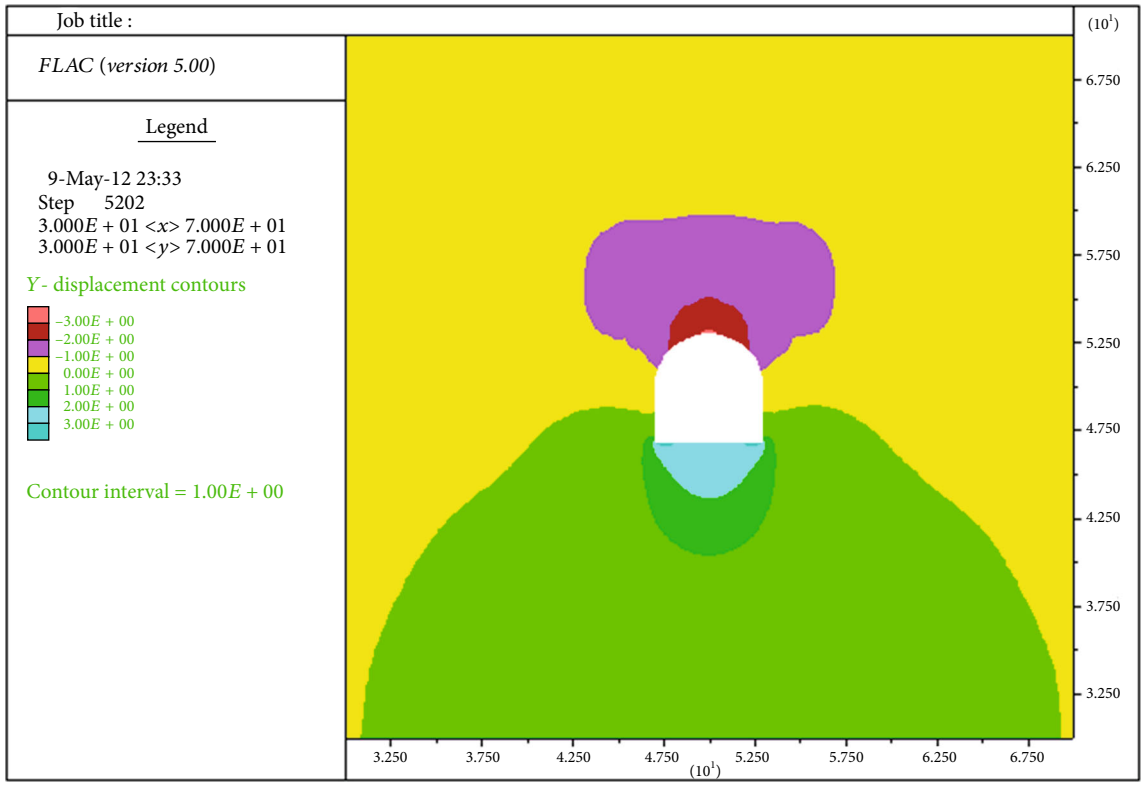

Vertical displacement

(b) Vertical displacement

Figure 10: Continued.

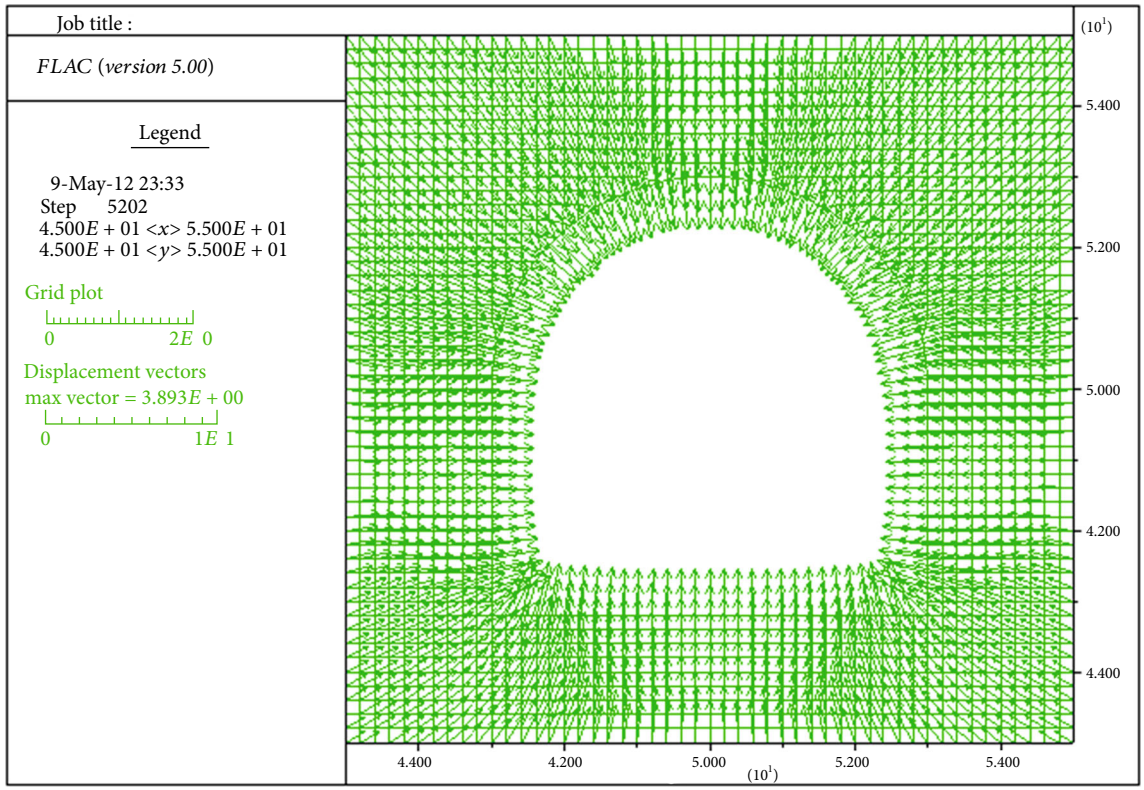

(c) Displacement vector

Figure 10: Movement rule of surrounding rock in the original support scheme.

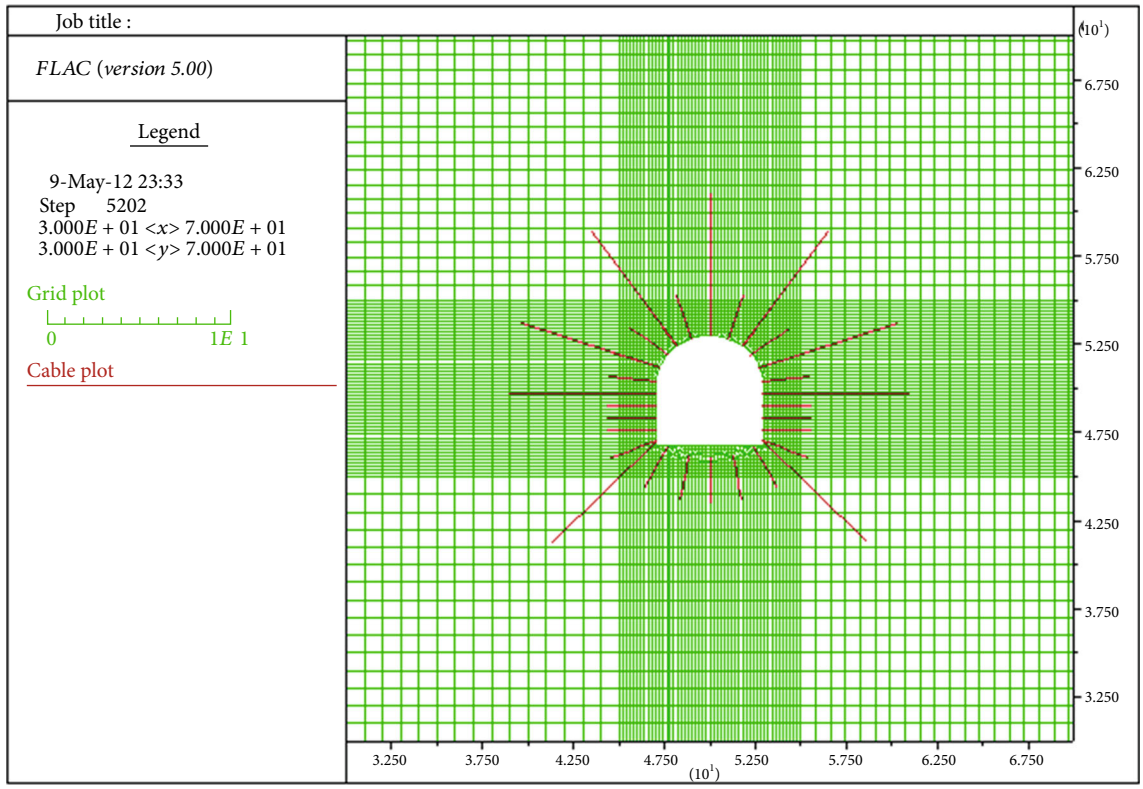

Figure 11: Calculation model of the MPC restoration support scheme.

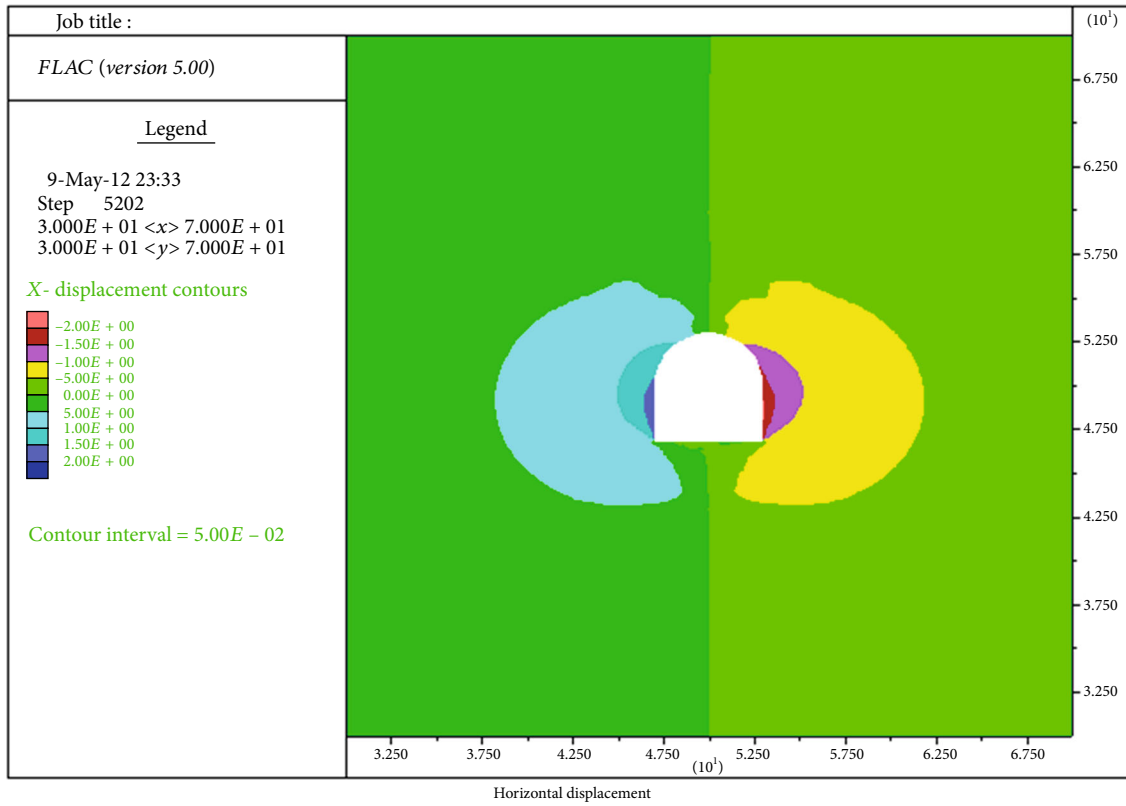

Horizontal displacement

(a) Horizontal displacement

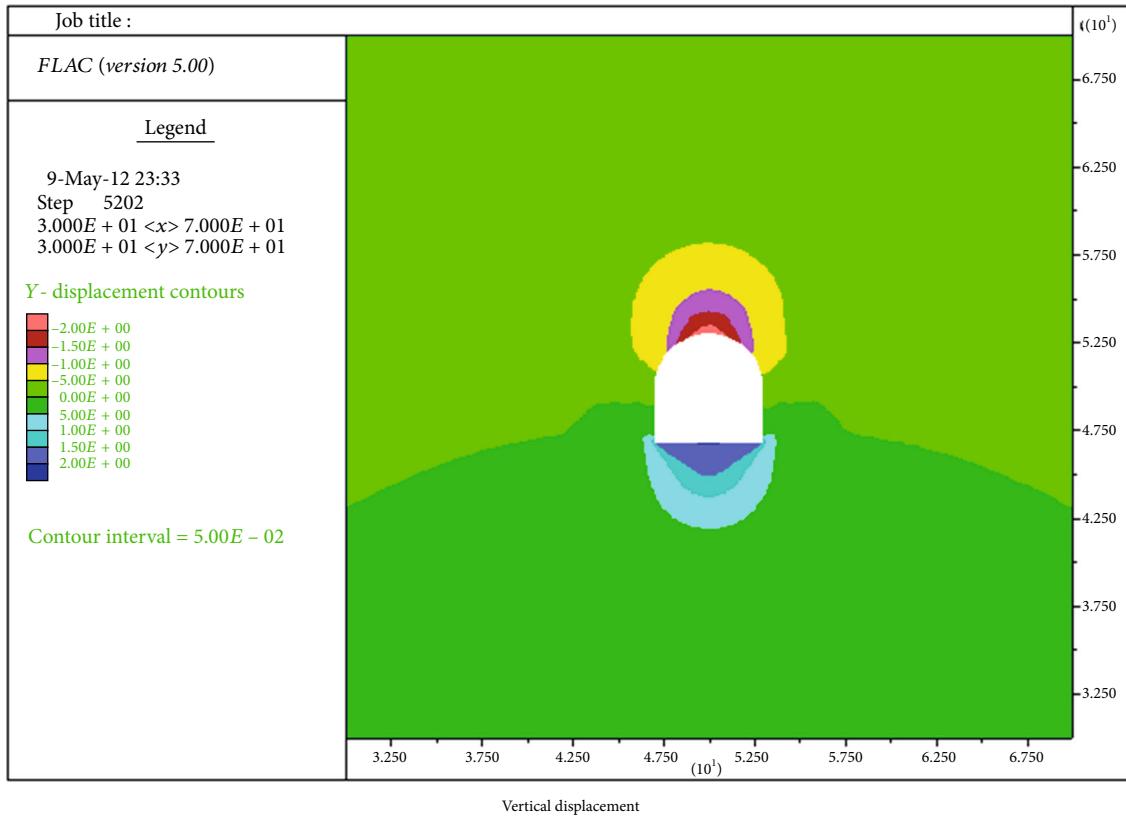

Vertical displacement

(b) Vertical displacement

Figure 12: Continued.

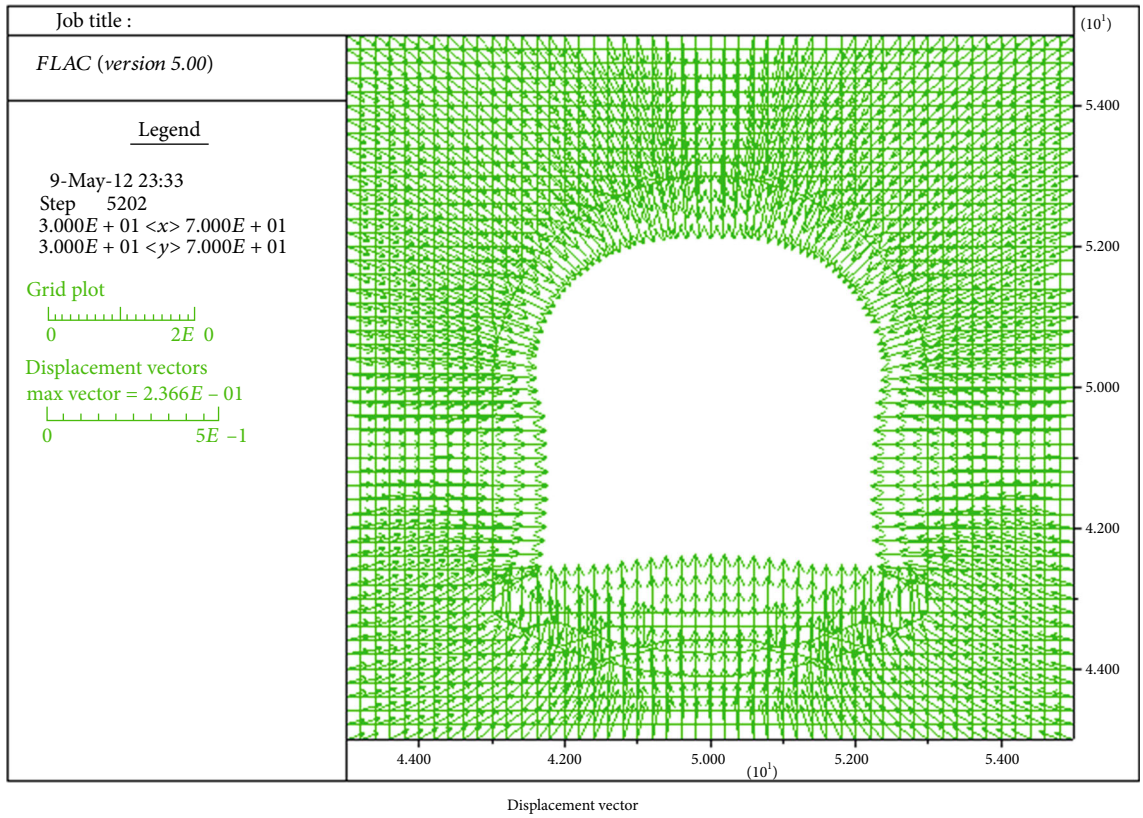

(c) Displacement vector

Figure 12: Movement rule of surrounding rock in a restoration scheme.

(1) The original support scheme: the chamber calculation model of the original support scheme is shown in Figure 9. After a certain number of steps in the iterative calculation, the distribution of deformation stress of MPC surrounding rock is shown in Figure 10 after the support of the original scheme. It can be seen that the deformation of each part of the chamber is larger than 2 m, which indicates that the chamber has been severely damaged and unstable, and within the calculation steps, it has not yet fully stabilized; from the distribution of stress and the plastic area around the chamber, the surrounding rock is in a large range of low-stress state, and the stress concentration around the chamber is apparent. Besides, the scope of the plastic zone is extensive, which is close to 3-4 times of roadway width. Therefore, the support scheme is not suitable for large chambers with the weak surrounding rock in high-stress areas, and the overall strength of the support structure and surrounding rock bearing body is low, which is unfavourable for the long-term stability of the roadway and prone to large deformation such as collapse.

(2) Repair plan: since the central pump house has been excavated for more than half a year and the deformation is relatively severe, the comprehensive treatment technology of "grouting+anchor bolt on the bottom plate+grouting anchor cable" is proposed based on the original support scheme. Therefore, the chamber calculation model is shown in Figure 11. After a certain number of steps of the iterative calculation, the displacement field distribution of MPC surrounding rock is shown in Figure 12 after the support of the restoration scheme. The deformation of each part is much smaller than that of the original scheme, in which the vault subsidence displacement is 236.6 mm, the sidewall deformation is 181.3 mm, and the floor heave is 214.4 mm. It shows that the restored scheme is conducive to the stability of the chamber, especially after grouting; it improves the integrity of the rock mass, enhances the bearing effect of support and surrounding rock, and achieves stability within the calculation steps; besides, due to the roof bolt support, the deformation of the floor is small. From the distribution of stress and the plastic area around the roadway, the range of stress release of surrounding rock is smaller, and the range of plastic area is much smaller than the original scheme, only close to about one time of the roadway width. Therefore, after the repair, the support scheme is beneficial to the stability of MPC in high-stress areas, improves the overall strength of the support structure and surrounding rock bearing body, and is conducive

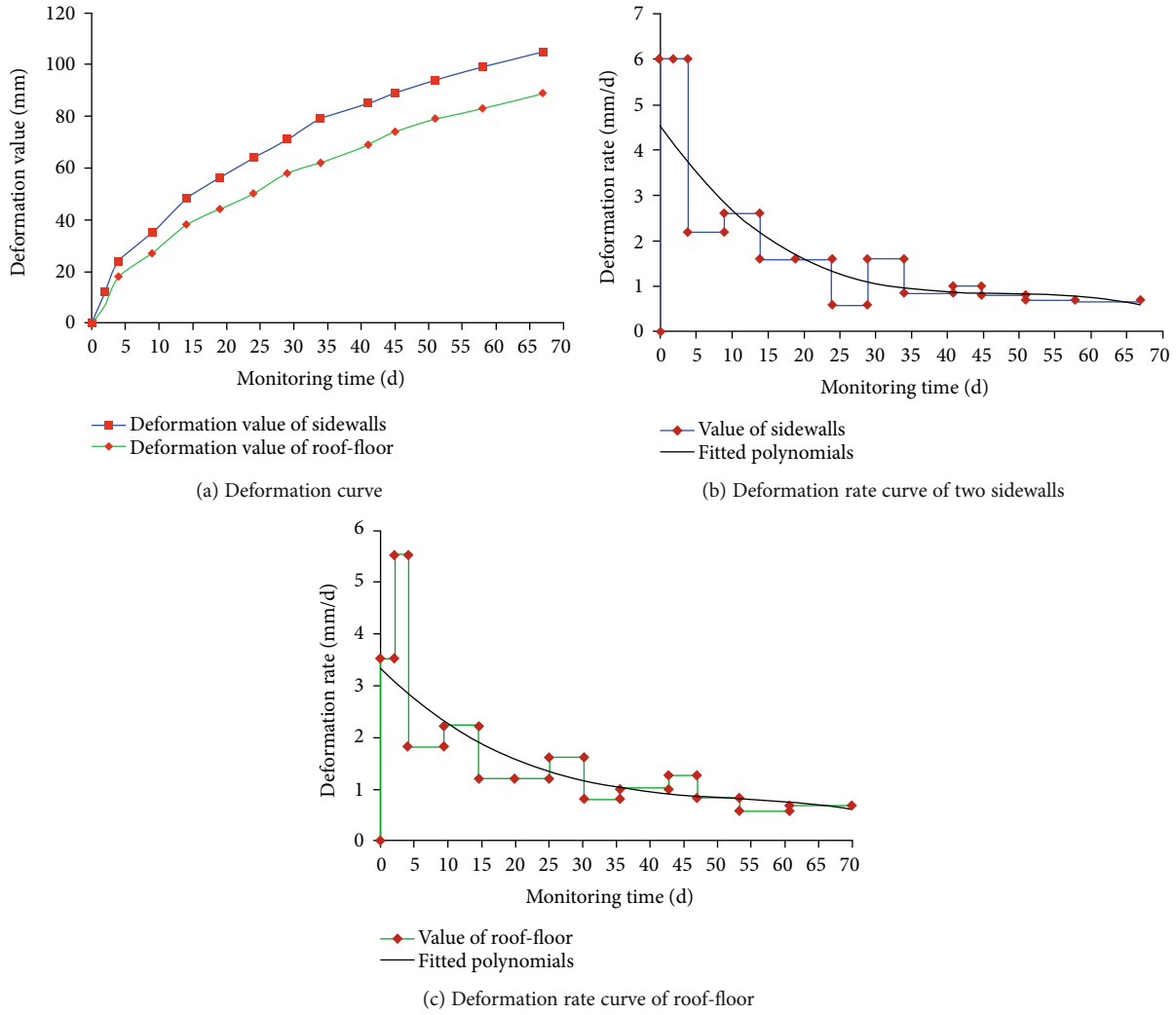

(a) Deformation curve

(b) Deformation rate curve of two sidewalls

(c) Deformation rate curve of roof-floor

Figure 13: Deformation monitoring curve after repair of MPC.

to maintaining the long-term stability of the chamber.

6.2. Control Effects of Designing Support Scheme on Site. Deformation monitoring of surrounding rock is shown in Figure 13 after the chamber adopts the repair scheme to strengthen the overall support of the whole section. It can be observed that the deformation of the surrounding rock of the chamber has been stable at this time. After 67 days, the two sidewalls are moved by 105 mm and the top and bottom plates by 89 mm. From the deformation rate of the two sidewalls and the top and bottom plates, the deformation rate is less than 0.7 mm/d in the later monitoring period and finally tends to be stable. Therefore, the comprehensive control technology of "bolt, metal mesh, shotcrete, grouting, anchor cable, and combined anchor cable" is beneficial to the long-term stability of the surrounding rock of deep large-span chambers.

7. Discussions

According to the survey data in this paper, the surrounding rock of CSC and MPC contains a lot of joints and fissures. The joint and fracture are treated as a whole with rock mass. Based on the Hoek-Brown failure criterion, the prediction model of mechanical parameters of rock mass affected by joints and fractures is established, and the prediction results are put into the numerical simulation software for calculation, so as to assist the support design. This is not a complex approach. At present, some researchers use DFN (Discrete Fracture Network), SRM (Synthetic Rock Mass), and other methods to reduce the joints and fissures obtained from field investigation directly in the numerical calculation model. Under the condition of accurately grasping the mechanical parameters of joints and fractures, this method is obviously more accurate than the method in this paper. However, it is difficult to accurately test the mechanical parameters of joints and fractures in the field. This method is still in the research stage, and the research results are not much. If there are mature results in the reconstruction of joints and fractures in the future, the reconstruction method is also recommended to study the jointed and fractured rock mass.

The Hoek-Brown failure criterion is empirical. Based on the criterion, a prediction model of rock mass parameters is established, so the prediction model is also an empirical

model. Some scholars are optimizing the Hoek-Brown criterion. After the failure criterion is optimized, the prediction model in this paper should also be optimized to make the prediction result closer to the engineering practice.

8. Conclusions

(1) The surrounding rock of the chambers is the typical whole section deformation feature with large deformation amount and duration, RMR of the surrounding rock of MPC is 54-61 (class III), and RMR of the surrounding rock of CSC is 35-42 (class IV). The surrounding rock is broken and contains clay minerals; the problem cannot be well-controlled by using the composite support scheme simply. The deformation of the chambers was characterized by a large amount of internal displacement of the sidewalls, severe floor heave, and long deformation time.

(2) The main idea of soft rock control in in-depth chamber engineering is to improve the strength of the surrounding rock of the inner structure as soon as possible and prevent the infinite relative displacement of concentrated stress in the surrounding rock. Six key points of support were proposed, which are to improve the initial support stiffness and strength of the support system, to give full play to the bearing function of the rock mass in the deep stable part, to expand the bearing area of the support system, to grasp the critical support stiffness of the support system accurately, to emphasize the combined support structure, and to improve the antideformation ability of the floor.

(3) The comprehensive support and repair scheme of "bolt, metal mesh, shotcrete, grouting, anchor cable, and combined anchor cable" is put forward, and the anchor support at the bottom angle is emphasized. The concrete repair process of the chamber is put forward. The numerical calculation and field monitoring data show that the restored support scheme is beneficial to the chamber's stability in the high-stress area; the scheme improves the overall strength of the support structure and surrounding rock-bearing body and is conducive to maintaining the long-term stability of the chambers.

Data Availability

The data used to support the findings of this study are included within the article.

Conflicts of Interest

All the authors declare that they have no known conflicts of interest that could influence the work reported in this paper.

Acknowledgments

This research was supported by the National Natural Science Foundation of China (No. 51974117) and the Hunan Provincial Natural Science Foundation of China (No. 2020JJ4027). Dr. Genshui Wu of China University of Mining and Technology (Beijing) had provided a lot of valuable opinions on the revision. We would like to express our sincere thanks to Dr. Wu.

References

[1] X. T. Feng, *Rock Mechanics and Engineering Volume 4,Excavation, Support and Monitoring*, CRC Press, England, 2016.

[2] J. A. Hudson and X. T. Feng, *Rock Engineering Risk*, CRC Press, Great Britain, 2015.

[3] M. Kanji, M. C. He, and L. R. Sousa, *Soft Rock Mechanics and Engineering*, Springer, Switzerland, 2020.

[4] W. J. Yu, B. Pan, F. Zhang, S. F. Yao, and F. F. Liu, "Deformation characteristics and determination of optimum supporting time of alteration rock mass in deep mine," *KSCE Journal of Civil Engineering*, vol. 23, no. 11, pp. 4921–4932, 2019.

[5] J. P. Zuo and J. Y. Shen, *The Hoek-Brown Failure Criterion-from Theory to Application*, Springer, Singapore, 2020.

[6] J. P. Zuo, J. T. Wang, and Y. Q. Jiang, "Macro/meso failure behavior of surrounding rock in deep roadway and its control technology," *International Journal of Coal Science & Technology*, vol. 6, no. 3, pp. 301–319, 2019.

[7] H. P. Kang, "Support technologies for deep and complex roadways in underground coal mines: a review," *International Journal of Coal Science & Technology*, vol. 1, no. 3, pp. 261–277, 2014.

[8] G. S. Wu, W. J. Yu, J. P. Zuo, C. Y. Li, J. H. Li, and S. H. Du, "Experimental investigation on rockburst behavior of the rock-coal-bolt specimen under different stress conditions," *Scientific Reports*, vol. 10, no. 1, 2020.

[9] Z. J. Wen, S. L. Jing, Y. J. Jiang et al., "Study of the fracture law of overlying strata under water based on the flow-stress-damage model," *Geofluids*, vol. 2019, Article ID 3161852, 12 pages, 2019.

[10] J. M. Galvin, *Ground Engineering*, Springer, Switzerland, 2016.

[11] O. Aydan, *Time-Dependency in Rock Mechanics and Rock Engineering*, CRC Press, Balkema, Croydon, 2017.

[12] Z. J. Wen, X. Wang, L. J. Chen, G. Lin, and H. L. Zhang, "Size effect on acoustic emission characteristics of coal-rock damage evolution," *Advances in Materials Science and Engineering*, vol. 2017, Article ID 3472485, 8 pages, 2017.

[13] H. P. Xie, "Research review of the state key research development program of China: deep rock mechanics and mining theory," *Journal of China Coal Society*, vol. 44, no. 5, pp. 1283–1305, 2019.

[14] M. C. He, "Progress and challenges of soft rock engineering in depth," *Journal of China Coal Society*, vol. 39, no. 8, pp. 1409–1417, 2014.

[15] S. C. Li, H. T. Wang, Q. Wang et al., "Failure mechanism of bolting support and high-strength bolt-grouting technology for deep and soft surrounding rock with high stress," *Journal of Central South University*, vol. 23, no. 2, pp. 440–448, 2016.

[16] S. C. Li, J. Zhang, Z. F. Li et al., "Investigation and practical application of a new cementitious anti-washout grouting

material," *Construction and Building Materials*, vol. 224, pp. 66–77, 2019.

[17] J. P. Zuo, Z. F. Wang, H. W. Zhou, J. L. Pei, and J. F. Liu, "Failure behavior of a rock-coal-rock combined body with a weak coal interlayer," *International Journal of Mining Science and Technology*, vol. 23, no. 6, pp. 907–912, 2013.

[18] H. P. Kang, Y. Z. Wu, and F. Q. Gao, "Deformation characteristics and reinforcement technology for entry subjected to mining-induced stresses," *Journal of Rock Mechanics and Geotechnical Engineering*, vol. 3, no. 3, pp. 207–219, 2011.

[19] H. P. Kang, P. F. Jiang, B. X. Huang et al., "Roadway strata control technology by means of bolting-modification destressing in synergy in 1 000 M deep coal mines," *Journal of China Coal Society*, vol. 45, no. 3, pp. 845–864, 2020.

[20] G. J. Wu, W. Z. Chen, S. P. Jia et al., "Deformation characteristics of a roadway in steeply inclined formations and its improved support," *International Journal of Rock Mechanics and Mining Sciences*, vol. 130, article 104324, 2020.

[21] G. J. Wu, S. P. Jia, W. Z. Chen, J. Q. Yuan, H. D. Yu, and W. S. Zhao, "An anchorage experimental study on supporting a roadway in steeply inclined geological formations," *Tunnelling and Underground Space Technology*, vol. 82, pp. 125–134, 2018.

[22] S. R. Xie, M. M. Gao, D. D. Chen et al., "Stability influence factors analysis and construction of a deep beam anchorage structure in roadway roof," *International Journal of Mining Science and Technology*, vol. 28, no. 3, pp. 445–451, 2018.

[23] S. R. Xie, E. P. Li, S. J. Li, J. G. Wang, C. C. He, and Y. F. Yang, "Surrounding rock control mechanism of deep coal roadways and its application," *International Journal of Mining Science and Technology*, vol. 25, no. 3, pp. 429–434, 2015.

[24] H. Yu, Z. Y. Niu, L. G. Kong, C. C. Hao, and P. Cao, "Mechanism and technology study of collaborative support with long and short bolts in large-deformation roadways," *International Journal of Mining Science and Technology*, vol. 25, no. 4, pp. 587–593, 2015.

[25] Y. L. Lu, L. G. Wang, and B. Zhang, "An experimental study of a yielding support for roadways constructed in deep broken soft rock under high stress," *Mining Science and Technology (China)*, vol. 21, no. 6, pp. 839–844, 2011.

[26] X. J. Tan, W. Z. Chen, H. Y. Liu et al., "A combined supporting system based on foamed concrete and U-shaped steel for underground coal mine roadways undergoing large deformations," *Tunnelling and Underground Space Technology*, vol. 68, pp. 196–210, 2017.

[27] Y. Z. Wu, H. P. Kang, J. X. Wu, and F. Q. Gao, "Deformation and support of roadways subjected to abnormal stresses," *Procedia Engineering*, vol. 26, pp. 665–674, 2011.

[28] R. S. Yang, Y. L. Li, D. M. Guo, L. Yao, T. M. Yang, and T. T. Li, "Failure mechanism and control technology of water-immersed roadway in high-stress and soft rock in a deep mine," *International Journal of Mining Science and Technology*, vol. 27, no. 2, pp. 245–252, 2017.

[29] L. G. Wang, Y. L. Lu, Y. G. Huang, and H. Y. Sun, "Deep-shallow coupled bolt-grouting support technology for soft rock roadway in deep mine," *Journal of China University of Mining and Technology*, vol. 45, no. 1, pp. 11–18, 2016.

[30] Q. B. Meng, L. J. Han, Y. Xiao, H. Li, S. Y. Wen, and J. Zhang, "Numerical simulation study of the failure evolution process and failure mode of surrounding rock in deep soft rock roadways," *International Journal of Mining Science and Technology*, vol. 26, no. 2, pp. 209–221, 2016.

[31] D. F. Zhu, Y. H. Wu, Z. H. Liu, X. Q. Dong, and J. Yu, "Failure mechanism and safety control strategy for laminated roof of wide-span roadway," *Engineering Failure Analysis*, vol. 111, article 104489, 2020.

[32] H. L. Zhang, J. J. Cao, and M. Tu, "Floor stress evolution laws and its effect on stability of floor roadway," *International Journal of Mining Science and Technology*, vol. 23, no. 5, pp. 631–636, 2013.

[33] F. Q. Gong, Wuxing Wu, Tianbin Li, and Xuefeng Si, "Experimental simulation and investigation of spalling failure of rectangular tunnel under different three-dimensional stress states," *International Journal of Rock Mechanics and Mining Sciences*, vol. 122, article 104081, 2019.

[34] X. B. Li, F. Q. Gong, M. Tao et al., "Failure mechanism and coupled static-dynamic loading theory in deep hard rock mining: a review," *Journal of Rock Mechanics and Geotechnical Engineering*, vol. 9, no. 4, pp. 767–782, 2017.

[35] G. Li, F. S. Ma, J. Guo, H. J. Zhao, and G. Liu, "Study on deformation failure mechanism and support technology of deep soft rock roadway," *Engineering Geology*, vol. 264, article 105262, 2020.

[36] R. Ulusay and J. A. Hudson, *The Complete ISRM Suggested Methods for Rock Characterization, Testing and Monitoring: 1974-2006*, ISRM Turkish National Group, Ankara, Turkey, 2007.

[37] W. J. Yu, G. S. Wu, and B. F. An, "Investigations of support failure and combined support for soft and fractured coal-rock tunnel in tectonic belt," *Geotechnical and Geological Engineering*, vol. 36, no. 6, pp. 3911–3929, 2018.